

REMARKS

Claims 1-11 are all the claims pending in the application.

I. Response to Nonstatutory Obviousness-type Double Patenting Rejection

Claims 1-11 are rejected on the ground of nonstatutory obviousness-type double patenting as allegedly being unpatentable over claim 1 of US Patent 7,250,226.

Applicants respectfully traverse the rejection.

It is respectfully submitted that claims 1-11 are not obvious based on claim 1 of US Patent 7,250,226 for the reasons of record and for the additional following reasons.

The Examiner asserts that since the patent shows that a broad class of triphenylamine monomer can be used to make the phosphorescent polymers (see col. 11, line 25), variations of this class would have been obvious to one of ordinary skill in the art.

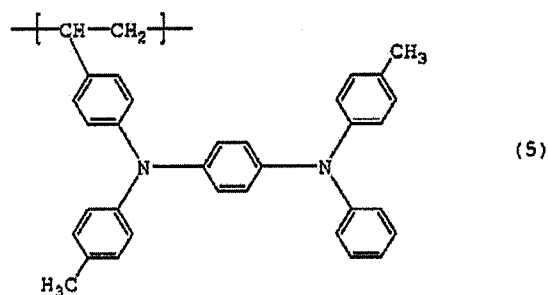
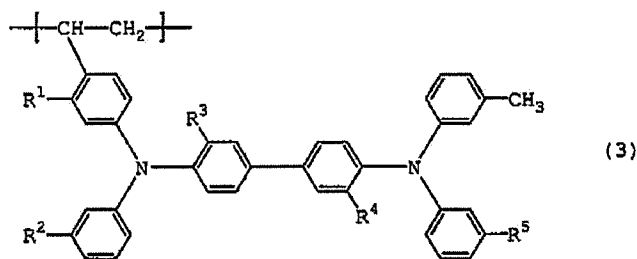
Applicants respectfully disagree for the reasons set forth below in Section II of the Remarks, submit that the present invention provides unexpectedly superior results as discussed in Section II, and request that the nonstatutory obviousness-type double patenting rejection be withdrawn.

II. Response to Rejection of Claims 1-7 under 35 U.S.C. § 103(a)

Claims 1-7 are rejected under 35 U.S.C. § 103(a) as allegedly being unpatentable over Tokito (2003/0091862).

Applicants respectfully traverse the rejection for the reasons of record and for the following additional reasons.

Claim 1 is directed to a phosphorescent polymer compound comprising a phosphorescent monomer unit and a monomer unit represented by the formula (3) or (5):



wherein R^1 to R^5 independently represent a hydrogen atom or a methyl group and at least one of R^1 and R^2 is a methyl group.

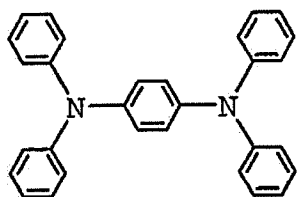
The Examiner asserts that the claimed formulas 3 and 5 only differ from the triphenylamine monomer of Tokito in (1) whether the spacer group between two nitrogen atoms is benzene or biphenyl and (2) whether it contains a methyl group as a substituent on some of the external phenyl rings. The Examiner considers that the differences in structure would not result in monomers that give rise to polymers with significantly different electronic properties.

Applicants respectfully disagree.

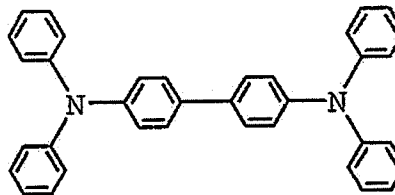
It is respectfully submitted that differences in the spacer group result in differences in electronic properties.

For example, Chemistry of Materials (vol. 10, 1998, pp 2235-2250), submitted herewith, describes electronic properties of triarylamine derivatives in which the spacer group between two nitrogen atoms is benzene or biphenyl. Table 1 (p. 2246) shows that DDP in which the

spacer group is benzene has the oxidation potential (V) relative to Ag/AgCl of 0.602V. Table 2 (p. 2247) shows that DDP in which the spacer group is biphenyl has the oxidation potential (V) relative to Ag/AgCl of 0.751V. That is, it is demonstrated that the difference in the spacer group will result in great differences in the oxidation potential value.

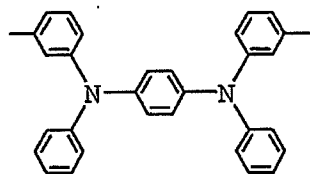


DDP
0.602V

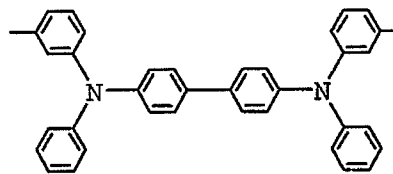


DDB
0.751V

Similarly, TTP in Table 1 in which the spacer group is benzene has the oxidation potential (V) of 0.561V while TPD (TTB) in Table 2 in which the spacer group is biphenyl has the oxidation potential (V) of 0.733V, which shows that the difference of the spacer group has great influence on the oxidation potential value.



TTP
0.561V



TPD (TTB)
0.733V

Thus, the Examiner's position that the difference in the spacer group would not result in monomers that give rise to polymers with significantly different electronic properties is not correct.

Additionally, DDP and DDB, and TTP and TPD greatly differ from each other regarding their values for the solution absorption spectra and the values for the solution fluorescence

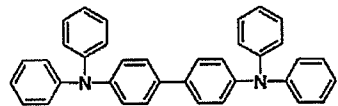
spectra (the values shown in the fourth and the last lines in each entry of Tables 1 and 2). It is therefore apparent that the differences in the spacer group do have a great influence on the electronic properties.

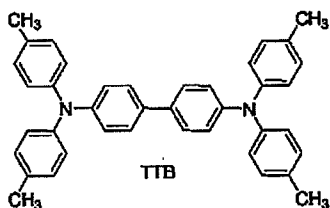
It is respectfully submitted that differences in the methyl substituent also result in differences in electronic properties.

For example, the only difference in the structure of DDP and TTP in Table 1 is the methyl substituent on the phenyl rings, however, DDP and TTP greatly differ in electronic properties such as oxidation potential value. Similarly, the only difference in the structure of DDB and TPD in Table 2 is the methyl substituent on the phenyl rings and the two greatly differ from each other in electronic properties.

Thus, the Examiner's position that the substitution of a methyl group would not result in monomers that give rise to polymers with significantly different electronic properties is not correct.

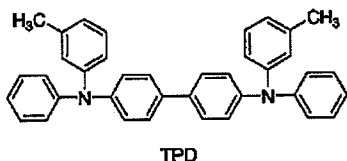
In addition, Advanced Functional Materials (vol. 16, 2006, pp 966-974), submitted herewith, discloses electronic properties of TPD and those of TAD and TTB, which differ from TPD in the methyl substituent. Tables 1 and 2 show the oxidation potential and hole mobility, respectively, and it can be seen that the difference in the number of the methyl substituents results in great difference in electronic properties of the compounds.

	E_{ox}	Hole mobility
 TAD	0.290V	6.7×10^{-5}



0.183V

1.8×10^{-5}



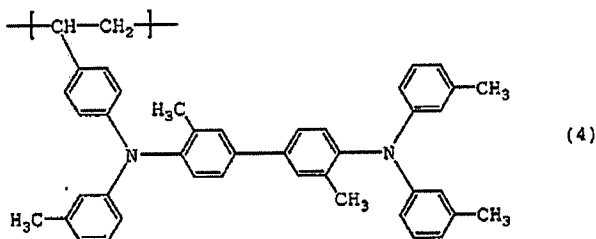
0.266V

8.7×10^{-5}

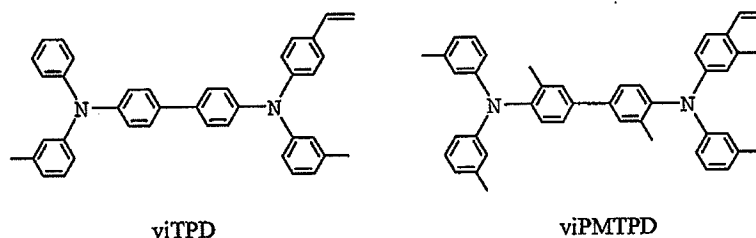
Accordingly, it is submitted that the differences in the structure between the monomer as taught by Tokito and the monomer of the present invention greatly influence the material properties and the performance of the organic EL element produced thereof.

As a result, the phosphorescent polymer of the present invention has unexpectedly superior effects compared to the polymer suggested by Tokito.

It is respectfully submitted that Example 3 and Example 4 should be compared and that Example 5 and Example 6 should be compared. The comparisons show the influence of the methyl substituent on the electronic properties of the polymer and unexpected superior results. Particularly, the unexpected results of when the phosphorescent monomer unit is represented by formula (4):



Specifically, Example 3 employs viTPD and Example 4 employs viPMPD (compound where the monomer is represented by formula (4)) as a hole transporting monomer unit. The difference in the monomer units is the methyl substituent.



As can be seen from Table 2 showing the results of Examples, the light emitting device of Example 4 has properties superior by 10 % or more in terms of the maximum luminance and external quantum efficiency compared to that of Example 3.

Similarly, a comparison of Example 5 (viTPD) and Example 6 (viPMPD) shows that the device of Example 6 has superior properties to that of Example 5 in terms of the maximum luminance and external quantum efficiency.

For at least the above reasons, it is respectfully submitted that Tokito discloses nor suggests the monomer unit represented by formula (3) or formula (5). It is also respectfully submitted that the present invention provides unexpectedly superior results, particularly the monomer of formula (4), in terms of luminance and efficiency of the organic EL device, that would not have been expected based on Tokito.

For at least the above reasons, it is respectfully submitted that claim 1 is patentable over Tokito.

Moreover, claims 2-7 depend from claim 1, and thus it is respectfully submitted that these claims are patentable for at least the same reasons as claim 1.

Accordingly, withdrawal of the rejection is respectfully requested.

III. Response to Rejection of Claims 8-11 under 35 U.S.C. § 103(a)

Claims 8-11 are still rejected under 35 U.S.C. § 103(a) as allegedly being unpatentable over Tokito and further in view of Hatwar (US Patent 6,127,004).

Applicants respectfully traverse the rejection.

It is respectfully submitted that since claims 8-11 depend from claim 1, these claims are patentable for at least the same reasons as claim 1. Accordingly, withdrawal of the rejection is respectfully requested.

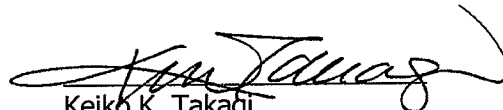
IV. Conclusion

In view of the above, reconsideration and allowance of claims 1-11 is respectfully requested.

If any points remain in issue which the Examiner feels may be best resolved through a personal or telephone interview, the Examiner is kindly requested to contact the undersigned at the telephone number listed below.

The USPTO is directed and authorized to charge all required fees, except for the Issue Fee and the Publication Fee, to Deposit Account No. 19-4880. Please also credit any overpayments to said Deposit Account.

Respectfully submitted,


Keiko K. Takagi
Registration No. 47,121

SUGHRUE MION, PLLC
Telephone: (202) 293-7060
Facsimile: (202) 293-7860

WASHINGTON OFFICE

23373

CUSTOMER NUMBER

Date: November 5, 2009

Asymmetric Triaryldiamines as Thermally Stable Hole Transporting Layers for Organic Light-Emitting Devices

Bryan E. Koene, Douglas E. Loy, and Mark E. Thompson*

Department of Chemistry, University of Southern California, Los Angeles, California 90089

Received March 24, 1998. Revised Manuscript Received June 1, 1998

The synthesis of a series of asymmetric triaryldiamines has provided a number of materials with a wide range of thermal, electrochemical, and spectroscopic properties. The asymmetric materials described herein have two different diarylamine groups bound to a 1,4-phenylene or 4,4'-biphenylene core, i.e., $\text{Ar}_1\text{Ar}_2\text{N}-\text{C}_6\text{H}_4-\text{NAr}_1'\text{Ar}_3$ or $\text{Ar}_1\text{Ar}_2\text{N-biphenyl-NAr}_1'\text{Ar}_3$, respectively. The diarylamines studied include diphenylamine, phenyl-*m*-tolylamine, naphthylphenylamine, iminostilbene, iminodibenzyl, and carbazole. These materials were prepared by copper- and palladium-catalyzed coupling of aryl halides and diarylamines. The asymmetry inherent in these compounds prevents these low molecular mass compounds from crystallizing, thus yielding higher thermal stability over that of the symmetric derivatives. In all cases, the asymmetric diamines form stable glasses, with glass transition temperatures up to 125 °C. HOMO levels for these materials, estimated by cyclic voltammetry, show a broad range of values, with oxidation potentials both lower and higher than those of common hole transport materials used in organic light emitting devices.

Introduction

Organic light emitting devices (OLEDs) have attracted a great deal of attention due to their potential use in a wide range of lighting as well as high- and low-resolution display applications. The first efficient organic light emitting device was fabricated as a single heterostructure device, using vacuum-deposited molecular thin films.¹ This OLED consisted of a structure constructed on an ITO (indium tin oxide) anode, with a tertiary amine hole transporting layer (HTL), an aluminum coordination complex electron-transporting layer (ETL), and the device was capped with a Mg–Ag cathode. A schematic diagram of this single heterostructure OLED along with the materials used to build the OLED is shown in Figure 1. A number of other materials and structures have been reported for OLEDs, but the basic mechanism for electroluminescence (EL) in most OLEDs is very similar. When a potential is applied across the OLED, holes are injected from the anode into the HTL and migrate in the presence of the electric field to the HTL/ETL interface. The applied potential also leads to injection of electrons from the cathode into the ETL and subsequent migration of these carriers to the ETL/HTL interface. The materials used for the transport layers are chosen carefully so that

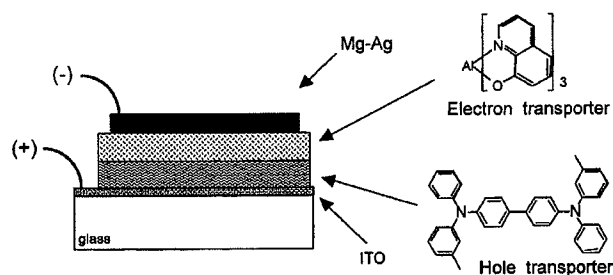


Figure 1. A schematic diagram of a single heterostructure OLED along with the structures of common materials used in OLEDs.

holes and electrons are preferentially conducted, but these materials do not conduct the opposite carrier to an appreciable extent. Thus, the HTL is both a hole conductor and an electron blocker and the ETL is both an electron conductor and a hole blocker. The proper choice of materials leads to a structure that confines the carriers in the organic materials and directs them to the HTL/ETL interface. Ideally, the holes and electrons recombine at or near the HTL/ETL interface to give excited molecules, or excitons, which radiatively relax to give the EL emission. The site of relaxation dictates the color of the EL emission, which can range from blue through the visible to the near-infrared depending on what materials are used to construct the OLED.²

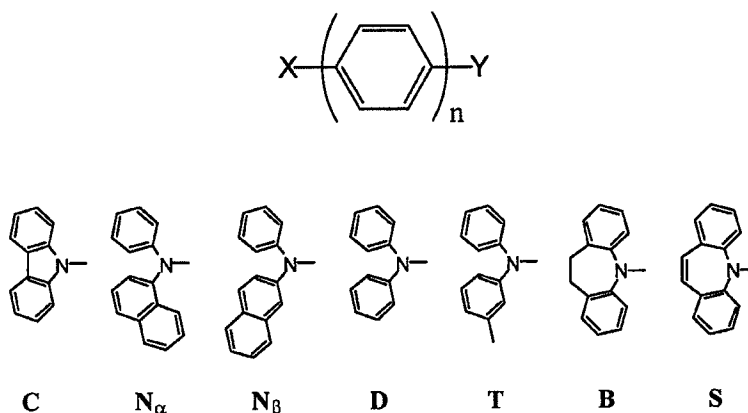
One of the principal failure modes in OLEDs involves thermal instability in the molecular thin films. There are a number of sources of thermal stress on the OLEDs. In the fabrication of the OLED, deposition of the metal cathode heats the organic heterostructure. During OLED operation, both joule heating, due to the insulating nature of the organic materials,^{3,4} and inefficient energy transfer in the devices contribute to the thermal

(1) Tang, C. W.; VanSlyke, S. A. *Appl. Phys. Lett.* **1987**, *51*, 913.

(2) Rothberg, L. J.; Lovinger, A. J. *J. Mater. Res.* **1996**, *11*, 3174.

Tang, C. W. *1996 SID Int. Symp., Digest of Technical Papers*; SID: San Diego, 1996; p 181. Tang, C. W. *Information Display* **1996**, *10*, 16. Sibley, S.; Thompson, M. E.; Burrows, P. E.; Forrest, S. R. In *Optoelectronic Properties of Inorganic Complexes*; Roundhill, D. M., Fakler, J., Eds.; Plenum Press: New York, in press. Shoustikov, A.; You, Y.; Thompson, M. E. *IEEE J. Spec. Top. Quantum Electron.*, in press. Burrows, P. E.; Gu, G.; Bulovic, V.; Forrest, S. R.; Thompson, M. E. *IEEE Trans. Electron. Dev.* **1997**, *44*, 1188. Forrest, S. R.; Burrows, P. E.; Thompson, M. E. In *Organic Electroluminescent Materials and Devices*; Miyata, S., Nalwa, H. S., Eds.; Gordon and Breach: New York, 1996.

Chart 1



Abbreviation	X	Y	n	Abbreviation	X	Y	n
TPD (TTB)*	T	T	2	$SN_\alpha B$	S	N_α	2
NPD ($N_\alpha N_\beta B$)*	N_α	N_β	2	$SN_\beta B$	S	N_β	2
CCB	C	C	2	SDB	S	D	2
DDP	D	D	1	STB	S	T	2
$N_\alpha N_\beta P$	N_α	N_β	1	SBB	S	B	2
CCP	C	C	1	SSB	S	S	2
BCB	B	C	2	$BN_\alpha B$	B	N_α	2
SCB	S	C	2	BBB	B	B	2
$N_\alpha CP$	N_α	C	1	$N_\alpha CB$	N_α	C	2
TCP	T	C	1	SCP	S	C	1

* Abbreviations in parentheses are the systematic names based on the definitions in this paper. They are referred to in the text, however, by their common abbreviations, also listed above.

stress on the OLED. If an OLED is heated above the glass transition temperature of one of the organic materials in the device, irreversible failure is observed. One model suggests that the failure may be related to significant expansion of the material that is observed at its T_g ,⁵ leading to significant disruption of the multilayer structure. In addition to irreversible degradation occurring above the T_g , it has been proposed that poor device lifetimes observed for devices operated near room temperature are partly due to thermal instabilities of the amorphous organic layers.^{6-8,176-8} The source of instability in these room temperature studies is thought to be dewetting and crystallization of the HTL materials, which occurs most readily in materials with comparatively low T_g s. In most OLED structures the HTL is the component with the lowest thermal stability. For example, the T_g for aluminum tris(8-hydroxyquinoline) (Alq), a common ETL, is 175 °C,⁹ while those for TPD and NPD (see Chart 1), common HTLs, are reported to be 65 and 95 °C, respectively.⁹

A considerable amount of research has focused on developing new materials for hole-transporting layers in OLEDs.⁹⁻²⁰ Several requirements must be fulfilled for these materials to be viable in their use as HTLs. The material must have a low barrier to hole injection from the anode, have a high hole mobility, a low barrier to hole injection into the ETL or emissive layer, and be thermally stable in an amorphous or glassy state. While it is easy to list the properties that a given material must have to be a useful HTL, it is not typically the case that all of these parameters are known for a given material before it is used in an OLED. The materials

- (3) Kuwahara, Y.; Ogawa, H.; Inada, H.; Noma, N.; Shirota, Y. *Adv. Mater.* **1994**, *6*, 677.
- (4) Adachi, C.; Nagai, K.; Tamoto, N. *Appl. Phys. Lett.* **1995**, *66*, 2679.
- (5) Fenter, P.; Schreiber, F.; Bulovic, V.; Forrest, S. R. *Chem. Phys. Lett.* **1997**, *277*, 521.
- (6) Adachi, C.; Tsutsui, T.; Saito, S. *Appl. Phys. Lett.* **1990**, *56*, 799.
- (7) Han, E.; Do, L.; Nijdom, Y.; Fujihira, M. *Chem. Lett.* **1994**, 969.
- (8) Tokito, S.; Taga, Y. *Appl. Phys. Lett.* **1995**, *66*, 673.

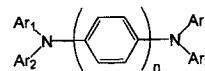
- (9) Naito, K.; Miura, A. *J. Phys. Chem.* **1993**, *97*, 6240.
- (10) Han, E.-M.; Do, L.-M.; Fujihira, M.; Inada, H.; Shirota, Y. *J. Appl. Phys.* **1996**, *80*, 3297.
- (11) Tokito, S.; Tanaka, H.; Okada, A.; Taga, Y. *Appl. Phys. Lett.* **1996**, *69*, 878.
- (12) Noda, T.; Imae, I.; Noma, N.; Shirota, Y. *Adv. Mater.* **1997**, *9*, 239.
- (13) Shirota, Y.; Kobata, T.; Noma, N. *Chem. Lett.* **1989**, 1145.
- (14) Noda, T.; Ogawa, H.; Noma, N.; Shirota, Y. *Appl. Phys. Lett.* **1997**, *70*, 699.
- (15) Inada, H.; Ohnishi, K.; Nomura, S.; Higuchi, A.; Nakano, H.; Shirota, Y. *J. Mater. Chem.* **1994**, *4*, 171.
- (16) Rommens, J.; Van der Auweraer, M.; De Schryver, F. C. *J. Phys. Chem. B* **1997**, *101*, 3081.
- (17) Van Slyke, S. A.; Chen, C. H.; Tang, C. W. *Appl. Phys. Lett.* **1996**, *69*, 2160.
- (18) Kido, J.; Komada, M.; Harada, G.; Nagai, K. *Polym. Adv. Technol.* **1995**, *17*, 703.
- (19) Higuchi, A.; Inada, H.; Kobata, T.; Shirota, Y. *Adv. Mater.* **1991**, *3*, 549.
- (20) Thayumanavan, S.; Barlow, S.; Marder, S. R. *Chem. Mater.* **1997**, *9*, 3231.

that have been found to have the best general match to the HTL requirements are triarylamines. These materials were well-known as hole conductors in xerographic applications long before they were used for OLEDs.²¹ One of the most widely used HTL materials in OLEDs is TPD (4,4'-bis(phenyl-*m*-tolylamino)biphenyl). TPD fulfills the first four requirements for an HTL, giving devices with excellent EL efficiencies and low turn-on voltages;²² however, the thermal stability is poor ($T_g = 65^\circ\text{C}$). In addition, although films of TPD are amorphous when deposited, they have been shown to crystallize in air at room temperature and at elevated temperatures ($60\text{--}80^\circ\text{C}$) in the absence of air.¹⁰ This crystallization contributes to device failure.

The main objective for developing new HTL materials is to improve the thermal properties while maintaining the desired properties exhibited by TPD. A wide variety of approaches has been used in the endeavor to fulfill these requirements. For example, "starburst" molecules having a triphenylamine core have demonstrated improved thermal stability.^{10,13,15,16} The addition of bulky groups to the phenyl rings of benzidine derivatives has yielded higher T_g materials as well as improved device lifetimes (e.g., NPD has a T_g of 95°C).^{11,17,20} Another approach involves the use of spiro linkages between traditional HTL materials, which uniformly increases T_g values.²³ A series of molecules with a thiophene bridge has exhibited reasonable thermal properties as an HTL as well as acting as a yellow emitter in devices.^{12,14} The incorporation of TPD into a polymer, such as polymethacrylamide, has also been shown to improve thermal stability.¹⁸ In most of these higher T_g HTL materials, the triaryllamine is asymmetrically substituted; i.e., the amine nitrogen is bound to three different aryl groups. Asymmetric substitution of the triaryllamine hinders crystallization, often leading to stable glasses. A simple example of this can be seen by comparing *N,N,N,N*-tetraphenylphenylenediamine (DDP in Chart 1) with the naphthyl-substituted derivative (N_aN_aP in Chart 1). DDP does not form a glass, but gives exclusively a crystalline material with a melting point of 290°C , while replacing one of the phenyl groups with a naphthyl group (forming N_aN_aP) gives a stable glass with a T_g of 68°C and a melting point of 182°C .

The study reported herein is aimed at improving the thermal and electronic properties of HTLs. We have prepared a large series of compounds with different triarylamines in order to probe how the thermal, oxidation, and electronic properties change by varying substituents. In this series, we have investigated a novel and systematic approach to increasing the T_g values of triarylamines. Some of the most efficient HTL materials are benzidine derivatives (4,4'-diaminobiphenyls), e.g., TPD and NPD. These materials are asymmetric in that they have three different aryl groups bound to each nitrogen atom (e.g., phenyl, naphthyl, and biphenyl for NPD), but the two nitrogen atoms are identically substituted. Our approach was to not only have materi-

Chart 2



als with three different aryl groups on each nitrogen but to have asymmetry in the amines on either side of the biphenyl group; e.g., see Chart 2, $Ar_1 Ar_2 Ar_3$, Ar_1 may or may not be the same as Ar_1' . This asymmetry gives materials of this type a high propensity for forming stable glasses. It is important to point out, however, that the goal is to increase the glass transition temperature of the materials by making the molecules structurally asymmetric, without creating significant electronic asymmetry in the molecule. Electronic asymmetry, resulting in significant ground-state dipole moments for the molecules, would be expected to act as local carrier traps.²⁴ In addition to describing the thermal properties of these materials, we will discuss the oxidation potentials and electronic spectra of these asymmetric diamines.

Synthesis

General Methods. All amines, aryl halides, Cu, K_2CO_3 , tris(dibenzylideneacetone)dipalladium (Pd_2dba_3), sodium *tert*-butoxide, diphenylphosphinoferrocene (dppf), and 18-crown-6 were used as purchased from Aldrich without further purification. Sodium *tert*-butoxide, Pd_2dba_3 , and dppf were stored and handled in a glovebox under nitrogen. Anhydrous toluene was purchased from Aldrich in Sure-Seal bottles or prepared by distilling reagent-grade toluene over sodium benzophenone.

Mass spectra were recorded on an HP 5973 mass spectrometer, using electron ionization at 70 eV. NMR spectra were measured on a Bruker AC 250 MHz spectrometer. The glass transition temperatures and melting points were measured using a TA Instruments 910 differential scanning calorimeter (DSC). The samples were heated at a rate of 20°C per minute and were cooled using the quench cooling accessory provided with the instrument. UV spectra were measured with $\sim 10\ \mu\text{M}$ solutions of each diamine with an AVIV 14DS UV spectrometer. Fluorescence studies were carried out on the same solutions of each diamine with a Photon Technology International fluorescence spectrometer. Lifetimes of each of the iminostilbene biphenyl derivatives were measured on degassed solutions using a PTI Timemaster lifetime system. Elemental analysis was provided by Atlantic Microlabs.

Elemental analyses were performed on several representative samples because of the numerous compounds with similar structures that were prepared. These were found, in general, to be slightly low in carbon content, likely due to carbonizing of the organics at the high temperatures required for the analysis of these thermally stable materials. Low-resolution MS and ^1H NMR confirm the identity and purity of the compounds. Many peaks in the NMR spectra exhibit nonfirst order coupling patterns due to the large number of aromatic protons with similar chemical shifts, and thus, the term multiplets (*m*) was often used. The number of peaks found on a given multiplet average well above 10. Coupling constants were measured and reported only when the multiplicity could be unambiguously determined.

Method 1. Palladium-Catalyzed Synthesis. The following reactions were carried out via procedures similar to those found in the literature.²⁵

Singly Substituted Phenyl and Biphenyl Halide Synthesis. A round-bottomed flask was charged with Pd_2dba_3 (0.015 equiv), dppf (0.0225 equiv), and NaO^tBu (1.5 equiv) in

(21) Klupfel, K.-W.; Sus, O.; Behmenburg, H.; Neugebauer, W. *US* 3,180,730, 1965.

(22) Stolka, M.; Yanus, J. F.; Pai, D. M. *J. Phys. Chem.* **1984**, *88*, 4707.

(23) Salbeck, J.; Yu, N.; Bauer, J.; Weissörtel, F.; Bestgen, H. *Synth. Met.* **1997**, *91*, 209–215.

(24) Heun, S.; Borsenberger, P. M. *Chem. Phys.* **1995**, *200*, 245.

(25) Driver, M. S.; Hartwig, J. F. *J. Am. Chem. Soc.* **1996**, *118*, 7217; Wolre, J. P.; Wagaw, S.; Buchwald, S. L. *J. Am. Chem. Soc.* **1996**, *118*, 7215.

a nitrogen glovebox. Anhydrous toluene was added, and the reaction was stirred for 15 min. The 1,4-dibromobenzene or 4,4'-dibromobiphenyl (3–5 equiv) was added against a stream of nitrogen and the reaction was stirred for another 15 min. The mixture was heated to reflux for 8–24 h following the addition of the diarylamine (1.0 equiv). The reaction progress was followed by TLC (hexane or hexane/ethyl acetate) and/or MS until the diarylamine could not be detected.

Asymmetric Triaryldiamine Synthesis. The same synthesis was employed to prepare the asymmetric triaryldiamines, except 1.0 equiv of the aryl bromide and 1.1 equiv of the diarylamine were used. The reaction progress was monitored by the loss of the aryl bromide.

Symmetric Triaryldiamine Synthesis. The same synthesis was employed to prepare the symmetric triaryldiamines except the amounts of the reagents were used: Pd₂dba₃ (0.030 equiv), dppf (0.045 equiv), NaO^tBu (3.0 equiv), 1,4-dibromobenzene or 4-4'-dibromobiphenyl (1.0 equiv), and diarylamine (2.1 equiv). The reaction progress was monitored by the loss of the diarylamine.

Purification. The reaction mixture was concentrated to dryness under reduced pressure, dissolved in minimal CHCl₃, and recrystallized with ethanol or hexanes. Very high purity products were required for our analyses and device fabrication. Therefore, all products were gradient sublimed, yielding in most cases a >99% pure product (as determined by MS and NMR). While the sublimation step increases the purity of the material significantly, the losses in sublimation decrease the yield by roughly 10–50%. It should be mentioned that it has since been found that the product could be also obtained by the sublimation of the crude reaction mixture in the absence of the recrystallization step with no noticeable loss of purity or yield. In the case of the singly substituted triarylamines, the excess 1,4-dibromobenzene or 4,4'-dibromobiphenyl was initially removed by sublimation at a lower temperature.

Method 2. Copper-Catalyzed Synthesis. The copper catalyzed reactions followed general Ullmann syntheses.²⁶

Singly Substituted Phenyl and Biphenyl Halide Synthesis. A round-bottomed flask was charged with Cu (1.0 equiv), 18-crown-6 (0.15 equiv), and K₂CO₃ (2 equiv). *o*-Dichlorobenzene, 1,4-diiodobenzene (or 4,4'-diiodobiphenyl) (3–5 equiv), and the diarylamine (1.0 equiv) were added against a stream of nitrogen. The mixture was heated to 180–200 °C for 16–48 h. Reaction progress was followed until the diarylamine could not be detected. At the end of the reaction, the mixture was filtered hot through silica. The *o*-dichlorobenzene was then removed in vacuo, and the crude product was purified as previously mentioned.

Asymmetric Triaryldiamine Synthesis. The same synthesis was employed to prepare the asymmetric triaryldiamines except 1.0 equiv of the aryl bromide and 1.1 equiv of the diarylamine were used. The reaction progress was monitored by the loss of the aryl iodide.

Symmetric Triaryldiamine Synthesis. The same synthesis was employed to prepare the symmetric triaryldiamines except the following amounts of the reagents were used: Cu (2.0 equiv), 18-crown-6 (0.15 equiv), K₂CO₃ (4.0 equiv) 1,4-diiodobenzene or 4-4'-diiodobiphenyl (1.0 equiv), and diarylamine (2.0 equiv). The reaction progress was monitored by the loss of the diarylamine.

Singly Substituted Phenyl Halides. *N*-(4-Bromophenyl)carbazole (BrCP). BrCP was synthesized from 1,4-dibromobenzene and carbazole using method 1, yielding ~65 g (70%): ¹H NMR (acetone-*d*₆) δ 8.24 (d, 2H, *J* = 7.7 Hz), 7.85 (d, 2H, *J* = 8.5 Hz), 7.60 (d, 2H, *J* = 8.5 Hz), 7.48–7.24 (m, 6H); GCMS *m/z* 323 (M⁺, 100), 321 (M⁺, 100), 241 (50), 121 (25).

***N*-(4-Bromophenyl)-1-naphthylphenylamine (BrN_αP).** BrN_αP was synthesized from 1,4-dibromobenzene and 1-naphthylphenylamine using method 1, yielding 1.9 g (59%): ¹H NMR (CDCl₃) δ 7.91 (d, 1H, *J* = 8.5 Hz), 7.81 (d, 1H, *J* = 8.3

Hz), 7.55–6.93 (m, ca. 12H), 6.88 (d, 2H, *J* = 9.3 Hz); MS *m/z* 375 (M⁺, 100), 373 (M⁺, 100), 293 (34), 216 (56), 127 (17), 77 (30).

***N*-(4-Bromophenyl)-2-naphthylphenylamine (BrN_βP).** BrN_βP was synthesized from 1,4-dibromobenzene and 2-naphthylphenylamine using method 1, yielding 1.9 g (59%): ¹H NMR (CDCl₃) δ 7.73 (t, 2H, *J* = 8.5 Hz), 7.58 (d, 1H, *J* = 7.8 Hz), 7.47–6.93 (m, ca. 13H); MS *m/z* 375 (M⁺, 97), 373 (M⁺, 97), 293 (40), 216 (100), 184 (46), 127 (36), 77 (93).

***N*-(4-Iodophenyl)diphenylamine (IDP).** IDP was synthesized from 1,4-diiodobenzene and diphenylamine using method 2, yielding 2.9 g (35%): ¹H NMR (CDCl₃) δ 7.34–6.87 (m, ca. 14H); MS *m/z* 371 (M⁺, 100), 243 (39), 167 (58), 166 (70), 77 (78).

***N*-(4-Bromophenyl)phenyl-*m*-tolylamine (BrTP).** BrTP was synthesized from *p*-bromiodobenzene and 3-methyldiphenylamine using method 2, yielding 2.6 g (30%): ¹H NMR (CDCl₃) δ 7.34–6.79 (m, ca. 13H), 2.24 (s, 3H); MS *m/z* 385 (M⁺, 59), 339 (100), 337 (100), 257 (75), 180 (66), 152 (31), 128 (47), 77 (60).

***N*-(4-Bromophenyl)iminostilbene (BrSP).** BrSP was synthesized from 1,4-dibromobenzene and iminostilbene using method 1, yielding 2.2 g (40%): ¹H NMR (CDCl₃) δ 7.58–7.28 (m, ca. 9H), 7.03 (d, 2H, *J* = 9.3 Hz), 6.80 (s, 1H), 6.10 (d, 2H, *J* = 8.5 Hz); MS *m/z* 349 (M⁺, 100), 347 (M⁺, 100), 267 (63), 192 (77), 178 (77), 134 (68).

Singly Substituted Biphenyl Halides. 4-Iodo-4-(carbazolyl)biphenyl (ICB). ICB was synthesized from 4,4'-diiodobiphenyl and carbazole using method 2, yielding about 6.4 g (64%): ¹H NMR (CDCl₃) δ 8.14 (d, 2H, *J* = 8.3 Hz), 7.82 (d, 2H, *J* = 8.5 Hz), 7.77 (d, 2H, *J* = 8.5 Hz), 7.63 (d, 2H, *J* = 8.5 Hz), 7.50–7.24 (m, 8H); MS *m/z* 445 (M⁺, 68), 318 (70), 241 (12), 166 (50), 152 (100).

4-Iodo-4'-(1-naphthylphenylamino)biphenyl (IN_αB). IN_αB was synthesized from 4,4'-diiodobiphenyl and 1-naphthylphenylamine using method 2, yielding about 4.9 g (42%): ¹H NMR (CDCl₃) δ 7.92 (d, 1H, *J* = 8.3 Hz), 7.88 (d, 1H, *J* = 9.0 Hz), 7.78 (d, 1H, *J* = 7.5 Hz), 7.68 (d, 2H, *J* = 8.5 Hz), 7.53–6.90 (m, ca. 15H); MS *m/z* 497 (M⁺, 31), 370 (9), 293 (17), 241 (18), 217 (40), 152 (30), 127 (32), 77 (100).

4-Iodo-4'-(2-naphthylphenylamino)biphenyl (IN_βB). IN_βB was synthesized from 4,4'-diiodobiphenyl and 2-naphthylphenylamine using method 2, yielding about 5.9 g (50%): ¹H NMR (CDCl₃) δ 7.73 (t, 4H, *J* = 8.3 Hz), 7.58 (d, 2H, *J* = 8.3 Hz), 7.47–6.94 (m, ca. 14H); MS *m/z* 497 (M⁺, 100), 370 (68), 293 (62), 241 (48), 217 (83), 152 (57), 127 (40), 77 (72).

4-Iodo-4'-diphenylaminobiphenyl (IDB). IDB was synthesized from 4,4'-diiodobiphenyl and diphenylamine using method 2, yielding ~5.7 g (54%): ¹H NMR (CDCl₃) δ 7.44–7.19 (m, ca. 14H); MS *m/z* 447 (M⁺, 100), 320 (16), 241 (19), 167 (15), 77 (21).

4-Iodo-4'-(phenyl-*m*-tolylamino)biphenyl (ITB). ITB was synthesized from 4,4'-diiodobiphenyl and 3-methyldiphenylamine using method 2, yielding about 2.0 g (46%): ¹H NMR (CDCl₃) δ 7.73 (d, 2H, *J* = 8.8 Hz), 7.41 (d, 2H, *J* = 8.5 Hz), 7.34–6.83 (m, ca. 13H), 2.27 (s, 3H); MS *m/z* 461 (M⁺, 2), 335 (100), 293 (10), 243 (10), 167 (12), 150 (20).

4-Iodo-4'-(iminodibenzyl)biphenyl (IBB). IBB was synthesized from 4,4'-diiodobiphenyl and iminodibenzyl using method 2, yielding ~2.2 g (40%): ¹H NMR (CDCl₃) δ 7.66 (d, 2H, *J* = 8.3 Hz), 7.46–7.16 (m, ca. 12H), 6.63 (dd, 2H, *J* = 8.6, 3.0 Hz), 3.00 (s, 4H); MS *m/z* 473 (M⁺, 22), 346 (16), 152 (100), 77 (42).

4-Bromo-4'-(iminostilbenyl)biphenyl (BrSB). ISB was synthesized from 4,4'-dibromobiphenyl and iminostilbene using method 1, yielding about 3.0 g (45%): ¹H NMR (CDCl₃) δ 7.52–7.15 (m, ca. 14H), 6.83 (s, 2H), 6.32 (d, 2H, *J* = 9.0 Hz); MS *m/z* 425 (M⁺, 100), 423 (M⁺, 100), 345 (34), 191 (47), 177 (28), 152 (40).

Asymmetric Phenyls. 1-Carbazolyl-4-(1-naphthylphenylamino)benzene (N_αCP). N_αCP was synthesized from *N*-(4-bromophenyl)carbazole (BrCP) and 1-naphthylphenylamine using method 1, yielding 0.72 g (50%): ¹H NMR (acetone-*d*₆) δ 8.18 (d, 2H, *J* = 7.5 Hz), 8.10–7.99 (m, 2H), 7.94 (d, 2H, *J* = 7.5 Hz), 7.67–7.12 (m, ca. 18H), 7.02 (t, 1H, *J* = 8.3 Hz);

(26) Gauthier, S.; Frechet, J. M. J. *Synthesis* **1987**, 383.

MS m/z 460 (M^+ , 100), 293 (30), 242 (13), 230 (M^{2+} , 57), 216 (26), 191 (12), 166 (21), 77 (6); abs λ_{\max} = 320, 350 nm; E_{mm} λ_{\max} = 416 nm.

1-Carbazolyl-4-(2-naphthylphenylamino)benzene ($N_{\beta}\text{CP}$). $N_{\beta}\text{CP}$ was synthesized from *N*-(4-bromophenyl)-carbazole (BrCP) and 2-naphthylphenylamine using method 1, yielding 1.02 g (71%): ^1H NMR (acetone- d_6) δ 8.20 (d, 2H, J = 7.5 Hz), 7.87 (t, 2H, J = 8.3 Hz), 7.73 (d, 2H, J = 8.3 Hz), 7.63–7.18 (m, ca. 17H), 7.10 (t, 1H, J = 7.5 Hz); MS m/z 460 (M^+ , 100), 293 (8), 242 (3), 230 (M^{2+} , 15), 216 (5), 166 (3), 77 (2); abs λ_{\max} = 285, 295, 320 nm; E_{mm} λ_{\max} = 409 nm.

1-Carbazolyl-4-(diphenylamino)benzene (DCP). DCP was synthesized from *N*-(4-bromophenyl)carbazole (BrCP) and diphenylamine using method 1, yielding 0.54 g (42%): ^1H NMR (acetone- d_6) δ 8.20 (d, 2H, J = 7.5 Hz), 7.53–7.05 (m, ca. 20H); MS m/z 410 (M^+ , 100), 243 (9), 241 (8), 205 (M^{2+} , 17), 166 (9), 77 (3); abs λ_{\max} = 295, 320 nm; E_{mm} λ_{\max} = 400 nm.

1-Carbazolyl-4-(phenyl-*m*-tolylamino)benzene (TCP). TCP was synthesized from *N*-(4-bromophenyl)carbazole (BrCP) and 3-methyldiphenylamine using method 1, yielding 0.83 g (63%): ^1H NMR (acetone- d_6) δ 8.13 (d, 2H, J = 7.5 Hz), 7.47–7.15 (m, ca. 15H), 6.89 (d, 1H, J = 7.8 Hz), 2.30 (s, 3H); MS m/z 424 (M^+ , 100), 258 (6), 241 (6), 212 (M^{2+} , 13), 181 (3), 166 (6); abs λ_{\max} = 295, 315 nm; E_{mm} λ_{\max} = 370 nm.

1-Carbazolyl-4-(iminodibenzyl)benzene (BCP). BCP was synthesized from *N*-(4-bromophenyl)carbazole (BrCP) and iminodibenzyl using method 1, yielding 0.96 g (71%): ^1H NMR (acetone- d_6) δ 8.17 (d, 2H, J = 7.8 Hz), 7.52 (d, 2H, J = 7.0 Hz), 7.48–7.16 (m, ca. 14H), 6.76 (d, 2H, J = 9.2 Hz), 3.08 (s, 4H); MS m/z 436 (M^+ , 100), 268 (5), 241 (7), 218 (13), 194 (10), 166 (3); abs λ_{\max} = 295 nm; E_{mm} λ_{\max} = 382 nm.

1-Carbazole-4-(iminostilbenyl)benzene (SCP). SCP was synthesized from *N*-(4-bromophenyl)carbazole (BrCP) and iminostilbene using method 1, yielding 0.75 g (56%): ^1H NMR (acetone- d_6) δ 8.14 (d, 2H, J = 7.5 Hz), 7.69–7.13 (m, ca. 16H), 6.99 (s, 2H), 6.44 (d, 2H, J = 9.2 Hz); MS m/z 434 (M^+ , 100), 268 (7), 255 (10), 242 (5), 217 (M^{2+} , 15), 192 (5), 165 (4); Abs λ_{\max} = 270, 300 nm; E_{mm} λ_{\max} = 393, 487 nm. Anal. Calcd for $\text{C}_{32}\text{H}_{22}\text{N}_2$: C, 88.45; H, 5.10; N, 6.45. Found: C, 87.53; H, 5.74; N, 6.32.

1-(1-Naphthylphenylamino)-4-(2-naphthylphenylamino)benzene ($N_{\beta}N_{\beta}\text{P}$). $N_{\beta}N_{\beta}\text{P}$ was synthesized from *N*-(4-bromophenyl)-1-naphthylphenylamine (Br $N_{\beta}\text{P}$) and 2-naphthylphenylamine using method 1, yielding 0.43 g (63%): ^1H NMR (CDCl_3) δ 7.96 (d, 1H, J = 8.3 Hz), 7.87 (d, 1H, J = 8.5 Hz), 7.81–6.83 (m, ca. 26H); MS m/z 512 (M^+ , 100), 385 (2), 293 (23), 256 (M^{2+} , 51), 217 (59), 191 (12), 127 (11), 77 (13); Abs λ_{\max} = 280, 320 nm; E_{mm} λ_{\max} = 399, 496 nm.

1-(1-Naphthylphenylamino)-4-(diphenylamino)benzene ($\text{DN}_{\beta}\text{P}$). $\text{DN}_{\beta}\text{P}$ was synthesized from *N*-(4-bromophenyl)-1-naphthylphenylamine (Br $N_{\beta}\text{P}$) and diphenylamine using method 1, yielding 0.48 g (77%): ^1H NMR (CDCl_3) δ 7.95 (d, 1H, J = 7.8 Hz), 7.87 (d, 1H, J = 7.5 Hz), 7.74 (d, 1H, J = 8.5 Hz), 7.52–6.79 (m, ca. 23H); MS m/z 462 (M^+ , 100), 293 (10), 242 (11), 217 (38), 167 (40), 127 (20), 77 (78); Abs λ_{\max} = 320 nm; E_{mm} λ_{\max} = 414, 501 nm.

1-(1-Naphthylphenylamino)-4-(phenyl-*m*-tolylamino)benzene ($\text{TN}_{\beta}\text{P}$). $\text{TN}_{\beta}\text{P}$ was synthesized from *N*-(4-bromophenyl)-1-naphthylphenylamine (Br $N_{\beta}\text{P}$) and 3-methyldiphenylamine using method 1, yielding 0.37 g (58%): ^1H NMR (CDCl_3) δ 7.95 (d, 1H, J = 8.5 Hz), 7.87 (d, 1H, J = 7.5 Hz), 7.75 (d, 1H, J = 8.5 Hz), 7.52–6.82 (m, ca. 21H), 6.77 (d, 1H, J = 7.8 Hz), 2.24 (s, 3H); MS m/z 476 (M^+ , 100), 293 (21), 257 (14), 238 (M^{2+} , 60), 217 (50), 167 (43), 127 (11), 77 (22); Abs λ_{\max} = 320 nm; E_{mm} λ_{\max} = 417, 506 nm.

1-(1-Naphthylphenylamino)-4-(iminodibenzyl)benzene ($\text{BN}_{\beta}\text{P}$). $\text{BN}_{\beta}\text{P}$ was synthesized from *N*-(4-bromophenyl)-1-naphthylphenylamine (Br $N_{\beta}\text{P}$) and iminodibenzyl using method 1, yielding 0.31 g (67%): ^1H NMR (CDCl_3) δ 7.93 (d, 1H, J = 7.8 Hz), 7.81 (d, 1H, J = 8.5 Hz), 7.67 (d, 1H, J = 7.5 Hz), 7.47–7.10 (m, ca. 15H), 6.90 (d, 2H, J = 8.5 Hz), 6.76 (d, 2H, J = 8.5 Hz), 6.45 (d, 2H, J = 8.8 Hz), 2.98 (s, 4H); MS m/z 488 (M^+ , 100), 308 (4), 294 (16), 268 (16), 244 (M^{2+} , 55), 217 (21), 194 (23), 127 (6), 77 (8); Abs λ_{\max} = 315 nm; E_{mm} λ_{\max} = 398, 510 nm.

1-(1-Naphthylphenylamino)-4-(iminostilbenyl)benzene ($\text{SN}_{\beta}\text{P}$). $\text{SN}_{\beta}\text{P}$ was synthesized from *N*-(4-bromophenyl)-iminostilbene (BrSP) and 1-naphthylphenylamine using method 1, yielding 0.44 g (63%): ^1H NMR (CDCl_3) δ 7.98 (d, 1H, J = 8.0 Hz), 7.90 (d, 1H, J = 7.5 Hz), 7.66 (d, 1H, J = 8.3 Hz), 7.59–6.65 (m, ca. 19H), 6.39 (d, 2H, J = 8.3 Hz), 6.19 (d, 2H, J = 8.8 Hz); MS m/z 486 (M^+ , 100), 293 (3), 267 (3), 243 (M^{2+} , 27), 192 (17), 127 (3), 77 (7); Abs λ_{\max} = 300, 350 nm; E_{mm} λ_{\max} = 407 nm.

1-(2-Naphthylphenylamino)-4-(diphenylamino)benzene ($\text{DN}_{\beta}\text{P}$). $\text{DN}_{\beta}\text{P}$ was synthesized from *N*-(4-bromophenyl)-2-naphthylphenylamine (BrPP) and diphenylamine using method 1, yielding 0.33 g (53%): ^1H NMR (CDCl_3) δ 7.71 (t, 2H, J = 9.2 Hz), 7.89 (d, 1H, J = 7.8 Hz), 7.44–6.93 (m, ca. 23H); MS m/z 462 (M^+ , 100), 385 (3), 293 (30), 243 (14), 231 (M^{2+} , 56), 217 (15), 167 (50), 127 (15), 77 (38); Abs λ_{\max} = 320 nm; E_{mm} λ_{\max} = 399, 475 (sh) nm.

1-(2-Naphthylphenylamino)-4-(phenyl-*m*-tolylamino)benzene ($\text{TN}_{\beta}\text{P}$). $\text{TN}_{\beta}\text{P}$ was synthesized from *N*-(4-bromophenyl)-2-naphthylphenylamine (Br $N_{\beta}\text{P}$) and 2-methyldiphenylamine using method 1, yielding 0.46 g (73%): ^1H NMR (CDCl_3) δ 7.72 (t, 2H, J = 8.5 Hz), 7.59 (d, 1H, J = 7.5 Hz), 7.44–6.87 (m, ca. 21H), 6.82 (d, 1H, J = 7.5 Hz), 2.27 (s, 3H); MS m/z 476 (M^+ , 100), 293 (28), 238 (M^{2+} , 58), 217 (56), 167 (55), 127 (13), 77 (23); abs λ_{\max} = 320 nm; E_{mm} λ_{\max} = 398, 470 nm.

1-(2-Naphthylphenylamino)-4-(iminodibenzyl)benzene ($\text{BN}_{\beta}\text{P}$). $\text{BN}_{\beta}\text{P}$ was synthesized from *N*-(4-bromophenyl)-2-naphthylphenylamine (Br $N_{\beta}\text{P}$) and iminodibenzyl using method 1, yielding 0.27 g (60%): ^1H NMR (CDCl_3) δ 7.76–6.85 (m, ca. 23H), 6.53 (d, 1H, J = 8.5 Hz), 3.03 (s, 4H); MS m/z 488 (M^+ , 100), 294 (10), 268 (10), 244 (M^{2+} , 36), 217 (20), 194 (23), 180 (13), 127 (8), 77 (9); Abs λ_{\max} = 280, 320 nm; E_{mm} λ_{\max} = 398, 475 nm.

1-(2-Naphthylphenylamino)-4-(iminostilbenyl)benzene ($\text{SN}_{\beta}\text{P}$). $\text{SN}_{\beta}\text{P}$ was synthesized from *N*-(4-bromophenyl)-iminostilbene (Br $N_{\beta}\text{P}$) and 2-naphthylphenylamine using method 1, yielding 0.35 g (50%): ^1H NMR (CDCl_3) δ 7.76 (d, 1H, J = 7.5 Hz), 7.60 (d, 1H, J = 8.3 Hz), 7.55–6.82 (m, ca. 20H), 6.79 (d, 2H, J = 9.0 Hz), 6.22 (d, 2H, J = 9.0 Hz); MS m/z 486 (M^+ , 100), 307 (5), 294 (4), 267 (4), 243 (M^{2+} , 14), 192 (14), 178 (4), 127 (4), 77 (4); Abs λ_{\max} = 280, 315 nm; E_{mm} λ_{\max} = 402 nm.

1-(Diphenylamino)-4-(phenyl-*m*-tolylamino)benzene (TDP). TDP was synthesized from *N*-(4-bromophenyl)phenyl-*m*-tolylamine (BrTP) and diphenylamine using method 1, yielding 0.35 g (59%): ^1H NMR (CDCl_3) δ 7.31–6.69 (m, ca. 23H), 2.25 (s, 3H); MS m/z 426 (M^+ , 100), 257 (5), 243 (4), 213 (M^{2+} , 19), 166 (40), 77 (18); Abs λ_{\max} = 315 nm; E_{mm} λ_{\max} = 397 nm.

1-(Diphenylamino)-4-(iminodibenzyl)benzene (BDP). BDP was synthesized from *N*-(4-iodophenyl)diphenylamine (IDP) and iminodibenzyl using method 1, yielding 0.30 g (50%): ^1H NMR (CDCl_3) δ 7.34–6.65 (m, ca. 20H), 6.65 (d, 2H, J = 8.6 Hz), 3.03 (s, 4H); MS m/z 438 (M^+ , 100), 360 (45), 219 (M^{2+} , 30).

1-(Diphenylamino)-4-(iminostilbenyl)benzene (SDP). SDP was synthesized from *N*-(4-bromophenyl)iminostilbene (BrDP) and diphenylamine using method 1, yielding 0.29 g (47%): ^1H NMR (CDCl_3) δ 7.51–6.70 (m, ca. 20H), 6.75 (d, 2H, J = 9.0 Hz), 6.20 (d, 2H, J = 8.3 Hz); MS m/z 436 (M^+ , 100), 359 (5), 268 (13), 257 (21), 218 (M^{2+} , 27), 192 (22), 178 (12), 77 (13); Abs λ_{\max} = 310 nm; E_{mm} λ_{\max} = 398 nm.

1-(Phenyl-*m*-tolylamino)-4-(iminodibenzyl)benzene (BTP). BTP was synthesized from *N*-(4-bromophenyl)phenyl-*m*-tolylamine (BrTP) and iminodibenzyl using method 1, yielding 0.36 g (58%): ^1H NMR (CDCl_3) δ 7.41 (d, 2H, J = 8.0 Hz), 7.32–6.65 (m, ca. 17H), 6.49 (d, 2H, J = 8.4 Hz), 3.01 (s, 4H), 2.21 (s, 3H); MS m/z 452 (M^+ , 38), 178 (100), 152 (37), 77 (92); Abs λ_{\max} = 320 nm; E_{mm} λ_{\max} = 398 nm.

1-(Phenyl-*m*-tolylamino)-4-(iminostilbenyl)benzene (STP). STP was synthesized from *N*-(4-bromophenyl)iminostilbene (BrTP) and 3-methyldiphenylamine using method 1, yielding 0.37 g (57%): ^1H NMR (CDCl_3) δ 7.55–6.80 (m, ca. 19H), 6.77 (d, 2H, J = 9.0 Hz), 6.19 (d, 2H, J = 9.0 Hz), 2.19

(s, 3H); MS m/z 450 (M^+ , 100), 271 (9), 257 (9), 225 (M^{2+} , 9), 192 (26), 178 (20), 165 (21), 77 (16); Abs λ_{\max} = 315 nm; E_{mm} λ_{\max} = 400 nm.

1-(Iminodibenzyl)-4-(iminostilbenyl)benzene (SBP). SBP was synthesized from *N*-(4-bromophenyl)iminostilbene (BrSP) and iminodibenzyl using method 1, yielding 0.38 g (57%): ^1H NMR (CDCl_3) δ 7.48–7.04 (m, ca. 16H), 6.78 (s, 2H), 6.33 (d, 2H, J = 9.0 Hz), 6.08 (d, 2H, J = 8.3 Hz), 2.93 (s, 4H); MS m/z 462 (M^+ , 100), 284 (15), 268 (33), 231 (M^{2+} , 60), 192 (52), 178 (39), 165 (32); Abs λ_{\max} = 310 nm; E_{mm} λ_{\max} = 395 nm. Anal. Calcd for $\text{C}_{34}\text{H}_{26}\text{N}_2$: C, 88.28; H, 5.67; N, 6.06. Found: C, 87.13; H, 5.57; N, 5.94.

Asymmetric Biphenyls. **4-Carbazoyl-4'-(1-naphthylphenylamino)biphenyl (N_aCB).** N_aCB was synthesized from 4-bromo-4'-(carbazoyl)biphenyl (BrCB) and 1-naphthylphenylamine using method 1, yielding 0.37 g (54%): ^1H NMR (CDCl_3) δ 8.21–6.92 (m, ca. 28H); MS m/z 536 (M^+ , 38), 342 (10), 240 (50), 216 (100), 165 (46), 126 (40), 76 (50); Abs λ_{\max} = 295, 320 nm; E_{mm} λ_{\max} = 422 nm.

4-Carbazoyl-4'-(2-naphthylphenylamino)biphenyl (N_bCB). N_bCB was synthesized from 4-bromo-4'-(carbazoyl)biphenyl (BrCB) and 2-naphthylphenylamine using method 1, yielding 0.41 g (61%): ^1H NMR (CDCl_3) δ 8.14 (d, 2H, J = 7.5 Hz), 7.82–7.16 (m, ca. 24H), 7.08 (t, 2H, J = 6.8 Hz); MS m/z 536 (M^+ , 100), 342 (8), 217 (62), 127 (32), 76 (25); Abs λ_{\max} = 295, 320, 345 nm; E_{mm} λ_{\max} = 404 nm.

4-Carbazoyl-4'-(diphenylamino)biphenyl (DCB). DCB was synthesized from 4-bromo-4'-(carbazoyl)biphenyl (BrCB) and diphenylamine using method 1, yielding 0.13 g (27%): ^1H NMR (CDCl_3) δ 8.22 (d, 2H, J = 7.0 Hz), 7.98 (d, 1H, J = 8.3 Hz), 7.91–7.18 (m, ca. 21H), 7.12 (t, 2H, J = 7.5 Hz); MS m/z 486 (M^+ , 100), 408 (2), 319 (7), 243 (M^{2+} , 37), 166 (4), 77 (2); Abs λ_{\max} = 295, 340 nm; E_{mm} λ_{\max} = 390 nm.

4-Carbazoyl-4'-(phenyl-*m*-tolylamino)biphenyl (TCB). TCB was synthesized from 4-bromo-4'-(carbazoyl)biphenyl (BrCB) and 3-methyldiphenylamine using method 1, yielding 0.35 g (70%): ^1H NMR (CDCl_3) δ 8.15 (d, 2H, J = 7.5 Hz), 7.78 (d, 2H, J = 8.3 Hz), 7.59 (d, 2H, J = 8.3 Hz), 7.55 (d, 2H, J = 9.0 Hz), 7.50–6.91 (m, ca. 16H), 6.88 (d, 1H, J = 7.5 Hz), 2.28 (s, 3H); MS m/z 500 (M^+ , 100), 333 (10), 318 (7), 250 (M^{2+} , 62), 166 (12); Abs λ_{\max} = 295, 345 nm; E_{mm} λ_{\max} = 400 nm.

4-Carbazoyl-4'-(iminodibenzyl)biphenyl (BCB). BCB was synthesized from 4-bromo-4'-(carbazoyl)biphenyl (BrCB) and iminodibenzyl using method 1, yielding 0.27 g (56%): ^1H NMR (CDCl_3) δ 8.14 (d, 2H, J = 7.5 Hz), 7.76–7.20 (m, ca. 20H), 6.70 (d, 2H, J = 8.5 Hz), 3.04 (s, 4H); MS m/z 512 (M^+ , 100), 256 (M^{2+} , 19), 194 (11), 167 (5), 152 (6); Abs λ_{\max} = 295, 325 nm; E_{mm} λ_{\max} = 373 nm. Anal. Calcd for $\text{C}_{40}\text{H}_{32}\text{N}_2$: C, 89.03; H, 5.51; N, 5.46. Found: C, 88.28; H, 5.36; N, 5.33.

4-Carbazoyl-4'-(iminostilbenyl)biphenyl (SCB). SCB was synthesized from 4-bromo-4'-(carbazoyl)biphenyl (BrCB) and iminostilbene using method 1, yielding 0.42 g (73%): ^1H NMR (CDCl_3) δ 8.14 (d, 2H, J = 7.5 Hz), 7.72–7.22 (m, ca. 20H), 6.87 (s, 2H), 6.41 (d, 2H, J = 8.5 Hz); MS m/z 510 (M^+ , 100), 343 (11), 332 (10), 315 (13), 255 (M^{2+} , 70), 192 (40), 178 (15), 166 (57), 152 (28), 139 (12); Abs λ_{\max} = 295, 315 nm; E_{mm} λ_{\max} = 386 nm. Anal. Calcd for $\text{C}_{38}\text{H}_{26}\text{N}_2$: C, 89.38; H, 5.13; N, 5.49. Found: C, 89.27; H, 5.07; N, 5.49.

4-(1-Naphthylphenylamino)-4'-(2-naphthylphenylamino)biphenyl ($\text{N}_a\text{N}_b\text{B}$). $\text{N}_a\text{N}_b\text{B}$ was synthesized from 4-iodo-4'-(1-naphthylphenylamino)biphenyl (IN_aB) and 2-naphthylphenylamine using method 2, yielding 0.45 g (38%): ^1H NMR (CDCl_3) δ 7.94 (d, 1H, J = 7.8 Hz), 7.87 (d, 1H, J = 7.8 Hz), 7.81–6.86 (m, ca. 30H); MS m/z 588 (M^+ , 100), 369 (3), 294 (M^{2+} , 40), 217 (27), 77 (5); Abs λ_{\max} = 340 nm; E_{mm} λ_{\max} = 431 nm.

4-(1-Naphthylphenylamino)-4'-(diphenylamino)biphenyl (DN_aB). DN_aB was synthesized from 4-iodo-4'-(1-naphthylphenylamino)biphenyl (IN_aB) and diphenylamine using method 2, yielding 0.28 g (43%): ^1H NMR (CDCl_3) δ 7.95 (d, 1H, J = 7.8 Hz), 7.88 (d, 1H, J = 7.8 Hz), 7.83–6.85 (m, ca. 28H); MS m/z 538 (M^+ , 100), 369 (3), 269 (M^{2+} , 34), 217 (9), 167 (8), 77 (3); Abs λ_{\max} = 310, 350 nm; E_{mm} λ_{\max} = 400 (sh), 450 nm.

4-(1-Naphthylphenylamino)-4'-(phenyl-*m*-tolylamino)biphenyl (TN_aB). TN_aB was synthesized from 4-iodo-4'-(1-naphthylphenylamino)biphenyl (IN_aB) and 3-methyldiphenylamine using method 2, yielding 0.24 g (36%): ^1H NMR (CDCl_3) δ 7.93 (d, 1H, J = 7.8 Hz), 7.86 (d, 1H, J = 7.8 Hz), 7.81–6.75 (m, ca. 27H), 2.15 (s, 3H); MS m/z 552 (M^+ , 100), 332 (1), 276 (M^{2+} , 25), 217 (7), 167 (5), 77 (3); Abs λ_{\max} = 315, 350 nm; E_{mm} λ_{\max} = 450 nm.

4-(1-Naphthylphenylamino)-4'-(iminodibenzyl)biphenyl (BN_aB). BN_aB was synthesized from 4-iodo-4'-(1-naphthylphenylamino)biphenyl (IN_aB) and iminodibenzyl using method 2, yielding 0.36 g (32%): ^1H NMR (CDCl_3) δ 7.96 (d, 1H, J = 7.6 Hz), 7.89 (d, 1H, J = 9.2 Hz), 7.82 (d, 1H, J = 8.4 Hz), 7.75 (d, 1H, J = 8.4 Hz), 7.55–6.82 (m, ca. 21H), 6.59 (d, 2H, J = 9.2 Hz), 2.99 (s, 4H); MS m/z 564 (M^+ , 100), 369 (5), 344 (3), 282 (M^{2+} , 37), 217 (16), 194 (21), 77 (5). Anal. Calcd for $\text{C}_{42}\text{H}_{32}\text{N}_2$: C, 89.33; H, 5.71; N, 4.96. Found: C, 88.55; H, 5.37; N, 4.55.

4-(1-Naphthylphenylamino)-4'-(iminostilbenyl)biphenyl (SN_aB). SN_aB was synthesized from 4-iodo-4'-(1-naphthylphenylamino)biphenyl (IN_aB) and iminostilbene using method 1, yielding 0.23 g (79%): ^1H NMR (CDCl_3) δ 7.91 (d, 1H, J = 7.6 Hz), 7.85 (d, 1H, J = 8.4 Hz), 7.73 (d, 1H, J = 7.6 Hz), 7.53–6.79 (m, ca. 25H), 6.29 (d, 2H, J = 9.2 Hz); MS m/z 562 (M^+ , 100), 281 (M^{2+} , 50), 217 (10), 192 (17), 165 (8); Abs λ_{\max} = 270, 330 nm; E_{mm} λ_{\max} = 404, 507 (br) nm. Anal. Calcd for $\text{C}_{42}\text{H}_{30}\text{N}_2$: C, 89.65; H, 5.37; N, 4.98. Found: C, 87.95; H, 5.32; N, 4.82.

4-(2-Naphthylphenylamino)-4'-(diphenylamino)biphenyl (DN_bB). DN_bB was synthesized from 4-iodo-4'-(diphenylamino)biphenyl (IDB) and 2-naphthylphenylamine using method 2, yielding 0.37 g (31%): ^1H NMR (CDCl_3) δ 7.81 (t, 2H, J = 8.4 Hz), 7.67 (d, 1H, J = 7.6 Hz), 7.58–7.03 (m, ca. 27H); MS m/z 538 (M^+ , 100), 369 (8), 269 (M^{2+} , 58), 217 (23), 167 (12), 77 (9); Abs λ_{\max} = 320, 350 nm; E_{mm} λ_{\max} = 417 nm.

4-(2-Naphthylphenylamino)-4'-(phenyl-*m*-tolylamino)biphenyl (TN_bB). TN_bB was synthesized from 4-iodo-4'-(2-naphthylphenylamino)biphenyl (IN_bB) and 3-methyldiphenylamine using method 2, yielding 0.49 g (44%): ^1H NMR (CDCl_3) δ 7.73 (t, 2H, J = 9.2 Hz), 7.59 (d, 1H, J = 8.4 Hz), 7.52–6.80 (m, ca. 26H), 2.26 (s, 3H); MS m/z 552 (M^+ , 100), 369 (10), 276 (M^{2+} , 95), 216 (76), 166 (47), 77 (40); Abs λ_{\max} = 320, 350 nm; E_{mm} λ_{\max} = 415 nm.

4-(2-Naphthylphenylamino)-4'-(iminodibenzyl)biphenyl (BN_bB). BN_bB was synthesized from 4-iodo-4'-(iminodibenzyl)biphenyl (IBB) and 2-naphthylphenylamine using method 2, yielding 0.27 g (25%): ^1H NMR (CDCl_3) δ 7.71 (t, 2H, J = 9.2 Hz), 7.57 (d, 1H, J = 9.2), 7.47–6.94 (m, ca. 23H), 6.62 (d, 2H, J = 9.2 Hz), 3.00 (s, 4H); MS m/z 564 (M^+ , 100), 368 (15), 296 (15), 282 (M^{2+} , 14), 217 (5), 77 (3); Abs λ_{\max} = 330 nm; E_{mm} λ_{\max} = 414 nm.

4-(2-Naphthylphenylamino)-4'-(iminostilbenyl)biphenyl (SN_bB). SN_bB was synthesized from 4-iodo-4'-(2-naphthylphenylamino)biphenyl (IN_bB) and iminostilbene using method 1, yielding 0.37 g (73%): ^1H NMR (CDCl_3) δ 7.81–6.95 (m, ca. 26H), 6.83 (s, 2H), 6.33 (d, 2H, J = 8.4 Hz); MS m/z 562 (M^+ , 100), 369 (3), 281 (M^{2+} , 32), 217 (13), 192 (18), 77 (3); Abs λ_{\max} = 280, 330 nm; E_{mm} λ_{\max} = 413, 518 (w, br) nm. Anal. Calcd for $\text{C}_{42}\text{H}_{30}\text{N}_2$: C, 89.65; H, 5.37; N, 4.98. Found: C, 89.54; H, 5.43; N, 4.87.

4-(Diphenylamino)-4'-(phenyl-*m*-tolylamino)biphenyl (TDB). TDB was synthesized from 4-iodo-4'-(diphenylamino)biphenyl (IDB) and 3-methyldiphenylamine using method 1, yielding 0.45 g (80%): ^1H NMR (CDCl_3) δ 7.48–6.80 (m, ca. 27H), 2.25 (s, 3H); MS m/z 502 (M^+ , 100), 333 (8), 319 (7), 251 (M^{2+} , 68), 167 (15), 77 (8); Abs λ_{\max} = 310, 350 nm; E_{mm} λ_{\max} = 396 nm.

4-(Diphenylamino)-4'-(iminodibenzyl)biphenyl (BDB). BDB was synthesized from 4-iodo-4'-(diphenylamino)biphenyl (IDB) and iminodibenzyl using method 1, yielding 0.26 g (51%): ^1H NMR (CDCl_3) δ 7.46–6.93 (m, ca. 24H), 6.62 (d, 2H, J = 9.2 Hz), 3.00 (s, 4H); MS m/z 514 (M^+ , 100), 257 (M^{2+} , 24), 194 (10), 167 (8), 77 (3); Abs λ_{\max} = 340 nm; E_{mm} λ_{\max} = 400 nm.

4-(Diphenylamino)-4'-(iminostilbenyl)biphenyl (SDB). SDB was synthesized from 4-bromo-4'-(iminostilbenyl)biphenyl (BrSB) and diphenylamine using method 1, yielding 0.64 g (53%): $^1\text{H NMR}$ (CDCl_3) δ 7.58–6.90 (m, ca. 24H), 6.83 (s, 2H), 6.31 (d, 2H, $J = 8.4$ Hz); MS m/z 512 (M^+ , 100), 256 (M^{2+} , 17), 192 (20), 192 (20), 178 (18), 165 (16), 152 (8), 77 (10); Abs $\lambda_{\text{max}} = 310$ (sh), 330 nm; $E_{\text{nm}} \lambda_{\text{max}} = 397, 513$ (br) nm.

4-(Phenyl-*m*-tolylamino)-4'-(iminodibenzyl)biphenyl (BTB). BTB was synthesized from 4-iodo-4'-(iminodibenzyl)biphenyl (IBB) and 3-methyldiphenylamine using method 2, yielding 0.28 g (25%): $^1\text{H NMR}$ (CDCl_3) δ 7.45–6.85 (m, ca. 22H), 6.80 (d, 1H, $J = 8.4$ Hz), 6.61 (d, 2H, $J = 8.4$), 2.99 (s, 4H), 2.23 (s, 3H); MS m/z 528 (M^+ , 67), 348 (17), 194 (66), 179 (74), 178 (100), 151 (38), 77 (32); Abs $\lambda_{\text{max}} = 340$ nm; $E_{\text{nm}} \lambda_{\text{max}} = 402$ nm.

4-(Phenyl-*m*-tolylamino)-4'-(iminostilbenyl)biphenyl (STB). STB was synthesized from 4-iodo-4'-(iminostilbene)biphenyl (ISB) and 3-methyldiphenylamine using method 1, yielding 0.55 g (44%): $^1\text{H NMR}$ (CDCl_3) δ 7.53–6.76 (m, ca. 25H), 6.31 (d, 2H, $J = 9.2$ Hz), 2.23 (s, 3H); MS m/z 526 (M^+ , 100), 263 (M^{2+} , 9), 193 (28), 178 (29), 152 (10), 77 (8); Abs $\lambda_{\text{max}} = 310$ (sh), 340 nm; $E_{\text{nm}} \lambda_{\text{max}} = 397, 517$ nm.

4-(Iminodibenzyl)-4'-(iminostilbenyl)biphenyl (SBB). SBB was synthesized from 4-iodo-4'-(iminostilbenyl)biphenyl (ISB) and iminodibenzyl using method 1, yielding 0.30 g (48%): $^1\text{H NMR}$ (CDCl_3) δ 7.08–7.56 (m, ca. 20H), 6.82 (s, 2H), 6.57 (d, 2H, $J = 8.4$ Hz), 6.29 (d, 2H, $J = 9.2$ Hz), 2.98 (s, 4H); MS m/z 538 (M^+ , 100), 344 (6), 269 (M^{2+} , 32), 194 (16), 192 (20), 178 (13), 165 (12); Abs $\lambda_{\text{max}} = 320$ nm; $E_{\text{nm}} \lambda_{\text{max}} = 411, 533$ (w,br) nm. Anal. Calcd for $\text{C}_{40}\text{H}_{30}\text{N}_2$: C, 89.19; H, 5.61; N, 5.20. Found: C, 88.14; H, 5.62; N, 5.10.

Symmetric Phenyls. 1,4-Bis(carbazolyl)benzene (CCP). CCP was synthesized from 1,4-dibromobenzene and carbazole using method 1, yielding 1.68 g (17%): $^1\text{H NMR}$ (CDCl_3) δ 8.18 (d, 4H, $J = 7.9$ Hz), 7.81 (s, 4H), 7.57 (d, 4H, $J = 8.5$ Hz), 7.47 (td, 4H, $J = 7.3, 1.2$ Hz), 7.33 (td, 4H, $J = 7.3, 1.2$ Hz); MS m/z 408 (M^+ , 100), 241 (4), 204 (M^{2+} , 50), 166 (8), 140 (8); Abs $\lambda_{\text{max}} = 295, 310$ nm; $E_{\text{nm}} \lambda_{\text{max}} = 343$ nm.

1,4-Bis(1-naphthylphenylamino)benzene ($\text{N}_a\text{N}_a\text{P}$). $\text{N}_a\text{N}_a\text{P}$ was synthesized from 1,4-diiodobenzene and 1-naphthylphenylamine using method 2, yielding 15.3 g (26%): $^1\text{H NMR}$ (acetone- d_6) δ 7.96 (d, 2H, $J = 9.2$ Hz), 7.84 (d, 2H, $J = 9.2$ Hz), 7.58–7.31 (m, 8H), 7.22–7.11 (m, 6H), 6.96 (s, 4H), 6.93–6.80 (m, 4H); MS m/z 512 (M^+ , 100), 293 (10), 256 (M^{2+} , 32), 217 (30); Abs $\lambda_{\text{max}} = 280, 320$ nm; $E_{\text{nm}} \lambda_{\text{max}} = 505$ nm.

1,4-Bis(2-naphthylphenylamino)benzene ($\text{N}_b\text{N}_b\text{P}$). $\text{N}_b\text{N}_b\text{P}$ was synthesized from 1,4-diiodobenzene and 2-naphthylphenylamine using method 2, yielding 2.15 g (52%): $^1\text{H NMR}$ (acetone- d_6) δ 7.81 (d, 4H, $J = 8.8$ Hz), 7.67 (d, 2H, $J = 7.8$ Hz), 7.49–7.25 (m, 12), 7.21–7.01 (m, 10H); MS m/z 512 (M^+ , 100), 368 (5), 293 (15), 256 (M^{2+} , 13), 217 (39), 191 (8), 127 (7), 77 (7); Abs $\lambda_{\text{max}} = 260, 280, 325$ nm; $E_{\text{nm}} \lambda_{\text{max}} = 471$ nm.

1,4-Bis(diphenylamino)benzene (DDP). DDP was synthesized from 1,4-dibromobenzene and diphenylamine using method 1, yielding 0.58 g (31%): $^1\text{H NMR}$ (CDCl_3) δ 7.32–7.22 (m, 8H), 7.10–6.96 (m, 16H); MS m/z 412 (M^+ , 100), 243 (9), 206 (M^{2+} , 9), 167 (44), 77 (30); Abs $\lambda_{\text{max}} = \text{nm}$; $E_{\text{nm}} \lambda_{\text{max}} = \text{nm}$.

1,4-Bis(phenyl-*m*-tolylamino)benzene (TTP). TTP was synthesized from 3-iodotoluene and $\text{N,N}'$ -diphenyl-1,4-phenylenediamine using method 2, yielding 2.66 g (76%): $^1\text{H NMR}$ (acetone- d_6) δ 7.31–6.81 (m, 22H), 2.33 (s, 6H); MS m/z 440 (M^+ , 100), 256 (10), 220 (M^{2+} , 26), 166 (32), 77 (8); Abs $\lambda_{\text{max}} = 315$ nm; $E_{\text{nm}} \lambda_{\text{max}} = 376$ nm.

1,4-Bis(iminodibenzyl)benzene (BBP). BBP was synthesized from 1,4-dibromobenzene and iminodibenzyl using method 1, yielding 0.55 g (11%): $^1\text{H NMR}$ (CDCl_3) δ 7.55–6.51 (m, 20H), 3.19 (s, 4H), 3.03 (s, 4H); MS m/z 464 (M^+ , 100), 232 (M^{2+} , 17), 194 (16), 165 (10); Abs $\lambda_{\text{max}} = 315$ nm; $E_{\text{nm}} \lambda_{\text{max}} = 368$ nm.

1,4-Bis(iminostilbenyl)benzene (SSP). SSP was synthesized from 1,4-dibromobenzene and iminostilbene using method 1, yielding 1.3 g (47%): $^1\text{H NMR}$ (CDCl_3) δ 7.52–7.27 (m, 16H), 6.81 (s, 4H), 5.88 (s, 4H); MS m/z 460 (M^+ , 100), 280

(10), 230 (M^{2+} , 13), 192 (11), 165 (8); Abs $\lambda_{\text{max}} = 290, 340$ nm; $E_{\text{nm}} \lambda_{\text{max}} = 444, 488$ nm.

Symmetric Biphenyls. 1,4-Bis(carbazolyl)biphenyl (CCB). CCB was synthesized from 4,4'-diiodobiphenyl and carbazole using method 2, yielding 8.25 g (85%): $^1\text{H NMR}$ (CDCl_3) δ 8.16 (d, 4H, $J = 7.7$ Hz), 7.91 (d, 4H, $J = 8.2$ Hz), 7.70 (d, 4H, $J = 8.2$ Hz), 7.57–7.26 (m, 12H); MS m/z 484 (M^+ , 100), 315 (7), 242 (M^{2+} , 54), 152 (7); Abs $\lambda_{\text{max}} = 255, 295, 320$ nm; $E_{\text{nm}} \lambda_{\text{max}} = 389$ nm.

1,4-Bis(1-naphthylphenylamino)biphenyl ($\text{N}_a\text{N}_b\text{B}$). $\text{N}_a\text{N}_b\text{B}$ was synthesized from 4,4'-dibromobiphenyl and 1-naphthylphenylamine using method 1, yielding 13.43 g (67%): $^1\text{H NMR}$ (CDCl_3) δ 7.75 (d, 2H, $J = 7.9$ Hz), 7.86 (d, 2H, $J = 7.9$ Hz), 7.75 (d, 2H, $J = 7.9$ Hz), 7.51–6.83 (m, 26H); MS m/z 588 (M^+ , 100), 294 (M^{2+} , 26), 217 (10); Abs $\lambda_{\text{max}} = 270, 340$ nm; $E_{\text{nm}} \lambda_{\text{max}} = 450$ nm.

1,4-Bis(2-naphthylphenylamino)biphenyl ($\text{N}_b\text{N}_b\text{B}$). $\text{N}_b\text{N}_b\text{B}$ was synthesized from 4,4'-dibromobiphenyl and 2-naphthylphenylamine using method 1, yielding 2.35 g (10%): $^1\text{H NMR}$ (CDCl_3) δ 7.80 (t, 4H, $J = 9.2$ Hz), 7.65 (d, 2H, $J = 7.9$ Hz), 7.59–7.17 (m, 24H), 7.11 (t, 2H, $J = 6.7$ Hz); MS m/z 588 (M^+ , 100), 369 (15), 294 (M^{2+} , 84), 217 (33), 242 (19), 191 (20), 115 (10); Abs $\lambda_{\text{max}} = 260, 300, 340$ nm; $E_{\text{nm}} \lambda_{\text{max}} = 450$ nm.

1,4-Bis(diphenylamino)biphenyl (DDB). DDB was synthesized from 4,4'-dibromobiphenyl and diphenylamine using method 1, yielding 4.14 g (45%): $^1\text{H NMR}$ (CDCl_3) δ 7.39–6.84 (m, 28H); MS m/z 488 (M^+ , 100), 319 (6), 244 (M^{2+} , 40), 167 (14), 77 (7); Abs $\lambda_{\text{max}} = 315$ (sh), 355 nm; $E_{\text{nm}} \lambda_{\text{max}} = 395$ nm.

1,4-Bis(phenyl-*m*-tolylamino)biphenyl (TTB). TTB was synthesized from 4,4'-dibromobiphenyl and 3-methyldiphenylamine using method 1, yielding 3.72 g (30%): $^1\text{H NMR}$ (CDCl_3) δ 7.43 (d, 4H, $J = 8.5$ Hz), 7.30–6.80 (m, 22H), 2.30 (s, 6H); MS m/z 516 (M^+ , 100), 333 (13), 258 (M^{2+} , 64), 167 (28), 77 (10); Abs $\lambda_{\text{max}} = 315, 355$ nm; $E_{\text{nm}} \lambda_{\text{max}} = 396$ nm.

1,4-Bis(iminodibenzyl)biphenyl (BBB). BBB was synthesized from 4,4'-dibromobiphenyl and iminodibenzyl using method 1, yielding 7.8 g (72%): $^1\text{H NMR}$ (acetone- d_6) δ 7.87 (d, 4H, $J = 8.8$ Hz), 7.64–6.17 (m, 8H), 3.03 (s, 4H), 2.99 (s, 4H); MS m/z 540 (M^+ , 100), 270 (M^{2+} , 16), 194 (10); Abs $\lambda_{\text{max}} = 320$ nm; $E_{\text{nm}} \lambda_{\text{max}} = 402$ nm.

1,4-Bis(iminostilbenyl)biphenyl (SSB). SSB was synthesized from 4,4'-dibromobiphenyl and iminostilbene using method 1, yielding 206 g (38%): $^1\text{H NMR}$ (CDCl_3) δ 7.53–7.26 (m, 16H), 7.06 (d, 4H, $J = 8.5$ Hz), 6.80 (s, 4H), 6.25 (d, 4H, $J = 8.5$ Hz); MS m/z 536 (M^+ , 100), 357 (11), 268 (M^{2+} , 72), 192 (52), 165 (30); Abs $\lambda_{\text{max}} = 300, 340$ (sh) nm; $E_{\text{nm}} \lambda_{\text{max}} = 530$ nm.

Singly Substituted Phenyl Halides. *N*-(4-Bromophenyl)-carbazole (BrCP). BrCP was synthesized from 1,4-dibromobenzene and carbazole using method 1, yielding about 65 g (70%): $^1\text{H NMR}$ (acetone- d_6) δ 8.24 (d, 2H), 7.85 (d, 2H), 7.60 (d, 2H), 7.48–7.24 (m, 6H); GCMS m/z 323 (M^+ , 100), 321 (M^+ , 100), 241 (50), 121 (25).

***N*-(4-Bromophenyl)-1-naphthylphenylamine (BrN_aP).** BrN_aP was synthesized from 1,4-dibromobenzene and 1-naphthylphenylamine using method 1, yielding 1.9 g (59%): $^1\text{H NMR}$ (CDCl_3) δ 7.91 (d, 1H), 7.81 (d, 1H), 7.55–6.93 (m, ca. 12H), 6.88 (d, 2H); MS m/z 375 (M^+ , 100), 373 (M^+ , 100), 293 (34), 216 (56), 127 (17), 77 (30).

***N*-(4-Bromophenyl)-2-naphthylphenylamine (BrN_bP).** BrN_bP was synthesized from 1,4-dibromobenzene and 2-naphthylphenylamine using method 1, yielding 1.9 g (59%): $^1\text{H NMR}$ (CDCl_3) δ 7.73 (t, 2H), 7.58 (d, 1H), 7.47–6.93 (m, ca. 13H); MS m/z 375 (M^+ , 97), 373 (M^+ , 97), 293 (40), 216 (100), 184 (46), 127 (36), 77 (93).

***N*-(4-Iodophenyl)diphenylamine (IDP).** IDP was synthesized from 1,4-diiodobenzene and diphenylamine using method 2, yielding 2.9 g (35%): $^1\text{H NMR}$ (CDCl_3) δ 7.34–6.87 (m, ca. 14H); MS m/z 371 (M^+ , 100), 243 (39), 167 (58), 166 (70), 77 (78).

***N*-(4-Bromophenyl)phenyl-*m*-tolylamine (BrTP).** BrTP was synthesized from *p*-bromiodobenzene and 3-methyldiphenylamine using method 2, yielding 2.6 g (30%): $^1\text{H NMR}$ (CDCl_3) δ 7.34–6.79 (m, ca. 13H), 2.24 (s, 3H); MS m/z 385

(M⁺, 59), 339 (100), 337 (100), 257 (75), 180 (66), 152 (31), 128 (47), 77 (60).

N-(4-Bromophenyl)iminostilbene (BrSP). BrSP was synthesized from 1,4-dibromobenzene and iminostilbene using method 1, yielding 2.2 g (40%): ¹H NMR (CDCl₃) δ 7.58–7.28 (m, ca. 9H), 7.03 (d, 2H), 6.80 (s, 1H), 6.11 (d, 2H); MS *m/z* 349 (M⁺, 100), 347 (M⁺, 100), 267 (63), 192 (77), 178 (77), 134 (68).

Singly Substituted Biphenyl Halides. 4-Iodo-4-(carbazolyl)biphenyl (ICB). ICB was synthesized from 4,4'-diiodobiphenyl and carbazole using method 2, yielding about 6.4 g (64%): ¹H NMR (CDCl₃) δ 8.14 (d, 2H), 7.82 (d, 2H), 7.77 (d, 2H), 7.63 (d, 2H), 7.50–7.24 (m, 8H); MS *m/z* 445 (M⁺, 68), 318 (70), 241 (12), 166 (50), 152 (100).

4-Iodo-4'-(1-naphthylphenylamino)biphenyl (IN_αB). IN_αB was synthesized from 4,4'-diiodobiphenyl and 1-naphthylphenylamine using method 2, yielding about 4.9 g (42%): ¹H NMR (CDCl₃) δ 7.92 (d, 1H), 7.88 (d, 1H), 7.78 (d, 1H), 7.68 (d, 2H), 7.53–6.90 (m, ca. 15H); MS *m/z* 497 (M⁺, 31), 370 (9), 293 (17), 241 (18), 217 (40), 152 (30), 127 (32), 77 (100).

4-Iodo-4'-(2-naphthylphenylamino)biphenyl (IN_βB). IN_βB was synthesized from 4,4'-diiodobiphenyl and 2-naphthylphenylamine using method 2, yielding about 5.9 g (50%): ¹H NMR (CDCl₃) δ 7.73 (t, 4H), 7.58 (d, 2H), 7.47–6.94 (m, ca. 14H); MS *m/z* 497 (M⁺, 100), 370 (68), 293 (62), 241 (48), 217 (83), 152 (57), 127 (40), 77 (72).

4-Iodo-4'-diphenylaminobiphenyl (IDB). IDB was synthesized from 4,4'-diiodobiphenyl and diphenylamine using method 2, yielding about 5.7 g (54%): ¹H NMR (CDCl₃) δ 7.44–7.19 (m, ca. 14H); MS *m/z* 447 (M⁺, 100), 320 (16), 241 (19), 167 (15), 77 (21).

4-Iodo-4'-(phenyl-*m*-tolylamino)biphenyl (ITB). ITB was synthesized from 4,4'-diiodobiphenyl and 3-methyldiphenylamine using method 2, yielding ~2.0 g (46%): ¹H NMR (CDCl₃) δ 7.73 (d, 2H), 7.41 (d, 2H), 7.34–6.83 (m, ca. 13H), 2.27 (s, 3H); MS *m/z* 461 (M⁺, 2), 335 (100), 293 (10), 243 (10), 167 (12), 150 (20).

4-Iodo-4'-(iminodibenzyl)biphenyl (IBB). IBB was synthesized from 4,4'-diiodobiphenyl and iminodibenzyl using method 2, yielding ~2.2 g (40%): ¹H NMR (CDCl₃) δ 7.66 (d, 2H), 7.46–7.16 (m, ca. 12H), 6.63 (dd, 2H), 3.00 (s, 4H); MS *m/z* 473 (M⁺, 22), 346 (16), 152 (100), 77 (42).

4-Bromo-4'-(iminostilbenyl)biphenyl (BrSB). ISB was synthesized from 4,4'-dibromobiphenyl and iminostilbene using method 1, yielding ~3.0 g (45%): ¹H NMR (CDCl₃) δ 7.52–7.15 (m, ca. 14H), 6.83 (s, 2H), 6.32 (d, 2H); MS *m/z* 425 (M⁺, 100), 423 (M⁺, 100), 345 (34), 191 (47), 177 (28), 152 (40).

Asymmetric Phenyls. 1-Carbazolyl-4-(1-naphthylphenylamino)benzene (N_αCP). N_αCP was synthesized from *N*-(4-bromophenyl)carbazole (BrCP) and 1-naphthylphenylamine using method 1, yielding 0.72 g (50%): ¹H NMR (acetone-*d*₆) δ 8.18 (d, 2H), 8.10–7.99 (m, 2H), 7.94 (d, 2H), 7.67–7.12 (m, ca. 18H), 7.02 (t, 1H); MS *m/z* 460 (M⁺, 100), 293 (30), 242 (13), 230 (M²⁺, 57), 216 (26), 191 (12), 166 (21), 77 (6); Abs λ_{max} = 320, 350 nm; E_{mm} λ_{max} = 416 nm.

1-Carbazolyl-4-(2-naphthylphenylamino)benzene (N_βCP). N_βCP was synthesized from *N*-(4-bromophenyl)carbazole (BrCP) and 2-naphthylphenylamine using method 1, yielding 1.02 g (71%): ¹H NMR (acetone-*d*₆) δ 8.20 (d, 2H), 7.87 (t, 2H), 7.73 (d, 2H), 7.63–7.18 (m, ca. 17H), 7.10 (t, 1H); MS *m/z* 460 (M⁺, 100), 293 (8), 242 (3), 230 (M²⁺, 15), 216 (5), 166 (3), 77 (2); Abs λ_{max} = 285, 295, 320 nm; E_{mm} λ_{max} = 409 nm.

1-Carbazolyl-4-(diphenylamino)benzene (DCP). DCP was synthesized from *N*-(4-bromophenyl)carbazole (BrCP) and diphenylamine using method 1, yielding 0.54 g (42%): ¹H NMR (acetone-*d*₆) δ 8.20 (d, 2H), 7.53–7.05 (m, ca. 20H); MS *m/z* 410 (M⁺, 100), 243 (9), 241 (8), 205 (M²⁺, 17), 166 (9), 77 (3); Abs λ_{max} = 295, 320 nm; E_{mm} λ_{max} = 400 nm.

1-Carbazolyl-4-(phenyl-*m*-tolylamino)benzene (TCP). TCP was synthesized from *N*-(4-bromophenyl)carbazole (BrCP) and 3-methyldiphenylamine using method 1, yielding 0.83 g (63%): ¹H NMR (acetone-*d*₆) δ 8.13 (d, 2H), 7.47–7.15 (m, ca. 15H), 6.89 (d, 1H), 2.30 (s, 3H); MS *m/z* 424 (M⁺, 100), 258

(6), 241 (6), 212 (M²⁺, 13), 181 (3), 166 (6); Abs λ_{max} = 295, 315 nm; E_{mm} λ_{max} = 370 nm.

1-Carbazolyl-4-(iminodibenzyl)benzene (BCP). BCP was synthesized from *N*-(4-bromophenyl)carbazole (BrCP) and iminodibenzyl using method 1, yielding 0.96 g (71%): ¹H NMR (acetone-*d*₆) δ 8.17 (d, 2H), 7.52 (d, 2H), 7.48–7.16 (m, ca. 14H), 6.76 (d, 2H), 3.08 (s, 4H); MS *m/z* 436 (M⁺, 100), 268 (5), 241 (7), 218 (13), 194 (10), 166 (3); Abs λ_{max} = 295 nm; E_{mm} λ_{max} = 382 nm.

1-Carbazole-4-(iminostilbenyl)benzene (SCP). SCP was synthesized from *N*-(4-bromophenyl)carbazole (BrCP) and iminostilbene using method 1, yielding 0.75 g (56%): ¹H NMR (acetone-*d*₆) δ 8.14 (d, 2H), 7.69–7.13 (m, ca. 16H), 6.99 (s, 2H), 6.44 (d, 2H); MS *m/z* 434 (M⁺, 100), 268 (7), 255 (10), 242 (5), 217 (M²⁺, 15), 192 (5), 165 (4); Abs λ_{max} = 270, 300 nm; E_{mm} λ_{max} = 393, 487 nm. Anal. Calcd for C₃₂H₂₂N₂: C, 88.45; H, 5.10; N, 6.45. Found: C, 87.53; H, 5.74; N, 6.32.

1-(1-Naphthylphenylamino)-4-(2-naphthylphenylamino)benzene (N_βN_αP). N_βN_αP was synthesized from *N*-(4-bromophenyl)-1-naphthylphenylamine (BrN_αP) and 2-naphthylphenylamine using method 1, yielding 0.43 g (63%): ¹H NMR (CDCl₃) δ 7.96 (d, 1H), 7.87 (d, 1H), 7.81–6.83 (m, ca. 26H); MS *m/z* 512 (M⁺, 100), 385 (2), 293 (23), 256 (M²⁺, 51), 217 (59), 191 (12), 127 (11), 77 (13); Abs λ_{max} = 280, 320 nm; E_{mm} λ_{max} = 399, 496 nm.

1-(1-Naphthylphenylamino)-4-(diphenylamino)benzene (DN_αP). DN_αP was synthesized from *N*-(4-bromophenyl)-1-naphthylphenylamine (BrN_αP) and diphenylamine using method 1, yielding 0.48 g (77%): ¹H NMR (CDCl₃) δ 7.95 (d, 1H), 7.87 (d, 1H), 7.74 (d, 1H), 7.52–6.79 (m, ca. 23H); MS *m/z* 462 (M⁺, 100), 293 (10), 242 (11), 217 (38), 167 (40), 127 (20), 77 (78); Abs λ_{max} = 320 nm; E_{mm} λ_{max} = 414, 501 nm.

1-(1-Naphthylphenylamino)-4-(phenyl-*m*-tolylamino)benzene (TN_αP). TN_αP was synthesized from *N*-(4-bromophenyl)-1-naphthylphenylamine (BrN_αP) and 3-methyldiphenylamine using method 1, yielding 0.37 g (58%): ¹H NMR (CDCl₃) δ 7.95 (d, 1H), 7.87 (d, 1H), 7.75 (d, 1H), 7.52–6.82 (m, ca. 21H), 6.77 (d, 1H), 2.24 (s, 3H); MS *m/z* 476 (M⁺, 100), 293 (21), 257 (14), 238 (M²⁺, 60), 217 (50), 167 (43), 127 (11), 77 (22); Abs λ_{max} = 320 nm; E_{mm} λ_{max} = 417, 506 nm.

1-(1-Naphthylphenylamino)-4-(iminodibenzyl)benzene (BN_αP). BN_αP was synthesized from *N*-(4-bromophenyl)-1-naphthylphenylamine (BrN_αP) and iminodibenzyl using method 1, yielding 0.31 g (67%): ¹H NMR (CDCl₃) δ 7.93 (d, 1H), 7.81 (d, 1H), 7.67 (d, 1H), 7.47–7.10 (m, ca. 15H), 6.90 (d, 2H), 6.76 (d, 2H), 6.45 (d, 2H), 2.98 (s, 4H); MS *m/z* 488 (M⁺, 100), 308 (4), 294 (16), 268 (16), 244 (M²⁺, 55), 217 (21), 194 (23), 127 (6), 77 (8); Abs λ_{max} = 315 nm; E_{mm} λ_{max} = 398, 510 nm.

1-(1-Naphthylphenylamino)-4-(iminostilbenyl)benzene (SN_αP). SN_αP was synthesized from *N*-(4-bromophenyl)-1-naphthylphenylamine (BrN_αP) and iminostilbene (BrSP) using method 1, yielding 0.44 g (63%): ¹H NMR (CDCl₃) δ 7.98 (d, 1H), 7.90 (d, 1H), 7.66 (d, 1H), 7.59–6.65 (m, ca. 19H), 6.39 (d, 2H), 6.19 (d, 2H); MS *m/z* 486 (M⁺, 100), 293 (3), 267 (3), 243 (M²⁺, 27), 192 (17), 127 (3), 77 (7); Abs λ_{max} = 300, 350 nm; E_{mm} λ_{max} = 407 nm.

1-(2-Naphthylphenylamino)-4-(diphenylamino)benzene (DN_βP). DN_βP was synthesized from *N*-(4-bromophenyl)-2-naphthylphenylamine (BrPP) and diphenylamine using method 1, yielding 0.33 g (53%): ¹H NMR (CDCl₃) δ 7.71 (t, 2H), 7.89 (d, 1H), 7.44–6.93 (m, ca. 23H); MS *m/z* 462 (M⁺, 100), 385 (3), 293 (30), 243 (14), 231 (M²⁺, 56), 217 (15), 167 (50), 127 (15), 77 (38); Abs λ_{max} = 320 nm; E_{mm} λ_{max} = 399, 475 (sh) nm.

1-(2-Naphthylphenylamino)-4-(phenyl-*m*-tolylamino)benzene (TN_βP). TN_βP was synthesized from *N*-(4-bromophenyl)-2-naphthylphenylamine (BrN_βP) and 3-methyldiphenylamine using method 1, yielding 0.46 g (73%): ¹H NMR (CDCl₃) δ 7.72 (t, 2H), 7.59 (d, 1H), 7.44–6.87 (m, ca. 21H), 6.82 (d, 1H), 2.27 (s, 3H); MS *m/z* 476 (M⁺, 100), 293 (28), 238 (M²⁺, 58), 217 (56), 167 (55), 127 (13), 77 (23); Abs λ_{max} = 320 nm; E_{mm} λ_{max} = 398, 470 nm.

1-(2-Naphthylphenylamino)-4-(iminodibenzyl)benzene (BN_βP). BN_βP was synthesized from *N*-(4-bromophenyl)-2-naphthylphenylamine (BrN_βP) and iminodibenzyl using

method 1, yielding 0.27 g (60%): ^1H NMR (CDCl_3) δ 7.76–6.85 (m, ca. 23H), 6.53 (d, 1H), 3.03 (s, 4H); MS m/z 488 (M^+ , 100), 294 (10), 268 (10), 244 (M^{2+} , 36), 217 (20), 194 (23), 180 (13), 127 (8), 77 (9); Abs λ_{max} = 280, 320 nm; E_{mm} λ_{max} = 398, 475 nm.

1-(2-Naphthylphenylamino)-4-(iminostilbenyl)benzene (SN_βP). SN_βP was synthesized from *N*-(4-bromophenyl)-iminostilbene (BrN_βP) and 2-naphthylphenylamine using method 1, yielding 0.35 g (50%): ^1H NMR (CDCl_3) δ 7.76 (d, 1H), 7.60 (d, 1H), 7.55–6.82 (m, ca. 20H), 6.79 (d, 2H), 6.22 (d, 2H); MS m/z 486 (M^+ , 100), 307 (5), 294 (4), 267 (4), 243 (M^{2+} , 14), 192 (14), 178 (4), 127 (4), 77 (4); Abs λ_{max} = 280, 315 nm; E_{mm} λ_{max} = 402 nm.

1-(Diphenylamino)-4-(phenyl-*m*-tolylamino)benzene (TDP). TDP was synthesized from *N*-(4-bromophenyl)phenyl-*m*-tolylamine (BrTP) and diphenylamine using method 1, yielding 0.35 g (59%): ^1H NMR (CDCl_3) δ 7.31–6.69 (m, ca. 23H), 2.25 (s, 3H); MS m/z 426 (M^+ , 100), 257 (5), 243 (4), 213 (M^{2+} , 19), 166 (40), 77 (18); Abs λ_{max} = 315 nm; E_{mm} λ_{max} = 397 nm.

1-(Diphenylamino)-4-(iminodibenzyl)benzene (BDP). BDP was synthesized from *N*-(4-iodophenyl)diphenylamine (IDP) and iminodibenzyl using method 1, yielding 0.30 g (50%): ^1H NMR (CDCl_3) δ 7.34–6.65 (m, ca. 20H), 6.65 (d, 2H), 3.03 (s, 4H); MS m/z 438 (M^+ , 100), 360 (45), 219 (M^{2+} , 30).

1-(Diphenylamino)-4-(iminostilbenyl)benzene (SDP). SDP was synthesized from *N*-(4-bromophenyl)iminostilbene (BrDP) and diphenylamine using method 1, yielding 0.29 g (47%): ^1H NMR (CDCl_3) δ 7.51–6.70 (m, ca. 20H), 6.75 (d, 2H), 6.20 (d, 2H); MS m/z 436 (M^+ , 100), 359 (5), 268 (13), 257 (21), 218 (M^{2+} , 27), 192 (22), 178 (12), 77 (13); Abs λ_{max} = 310 nm; E_{mm} λ_{max} = 398 nm.

1-(Phenyl-*m*-tolylamino)-4-(iminodibenzyl)benzene (BTP). BTP was synthesized from *N*-(4-bromophenyl)phenyl-*m*-tolylamine (BrTP) and iminodibenzyl using method 1, yielding 0.36 g (58%): ^1H NMR (CDCl_3) δ 7.41 (d, 2H), 7.32–6.65 (m, ca. 17H), 6.49 (d, 2H), 3.01 (s, 4H), 2.21 (s, 3H); MS m/z 452 (M^+ , 38), 178 (100), 152 (37), 77 (92); Abs λ_{max} = 320 nm; E_{mm} λ_{max} = 398 nm.

1-(Phenyl-*m*-tolylamino)-4-(iminostilbenyl)benzene (STP). STP was synthesized from *N*-(4-bromophenyl)iminostilbene (BrTP) and 3-methyldiphenylamine using method 1, yielding 0.37 g (57%): ^1H NMR (CDCl_3) δ 7.55–6.80 (m, ca. 19H), 6.77 (d, 2H), 6.19 (d, 2H), 2.19 (s, 3H); MS m/z 450 (M^+ , 100), 271 (9), 257 (9), 225 (M^{2+} , 9), 192 (26), 178 (20), 165 (21), 77 (16); Abs λ_{max} = 315 nm; E_{mm} λ_{max} = 400 nm.

1-(Iminodibenzyl)-4-(iminostilbenyl)benzene (SBP). SBP was synthesized from *N*-(4-bromophenyl)iminostilbene (BrSP) and iminodibenzyl using method 1, yielding 0.38 g (57%): ^1H NMR (CDCl_3) δ 7.48–7.04 (m, ca. 16H), 6.78 (s, 2H), 6.33 (d, 2H), 6.08 (d, 2H), 2.93 (s, 4H); MS m/z 462 (M^+ , 100), 284 (15), 268 (33), 231 (M^{2+} , 60), 192 (52), 178 (39), 165 (32); Abs λ_{max} = 310 nm; E_{mm} λ_{max} = 395 nm. Anal. Calcd for $\text{C}_{34}\text{H}_{26}\text{N}_2$: C, 88.28; H, 5.67; N, 6.06. Found: C, 87.13; H, 5.57; N, 5.94.

Asymmetric Biphenyls. 4-Carbazolyl-4'-(1-naphthylphenylamino)biphenyl (N_αCB). N_αCB was synthesized from 4-bromo-4'-(carbazolyl)biphenyl (BrCB) and 1-naphthylphenylamine using method 1, yielding 0.37 g (54%): ^1H NMR (CDCl_3) δ 8.21–6.92 (m, ca. 28H); MS m/z 536 (M^+ , 38), 342 (10), 240 (50), 216 (100), 165 (46), 126 (40), 76 (50); Abs λ_{max} = 295, 320 nm; E_{mm} λ_{max} = 422 nm.

4-Carbazolyl-4'-(2-naphthylphenylamino)biphenyl (N_βCB). N_βCB was synthesized from 4-bromo-4'-(carbazolyl)biphenyl (BrCB) and 2-naphthylphenylamine using method 1, yielding 0.41 g (61%): ^1H NMR (CDCl_3) δ 8.14 (d, 2H), 7.82–7.16 (m, ca. 24H), 7.08 (t, 2H); MS m/z 536 (M^+ , 100), 342 (8), 217 (62), 127 (32), 76 (25); Abs λ_{max} = 295, 320, 345 nm; E_{mm} λ_{max} = 404 nm.

4-Carbazolyl-4'-(diphenylamino)biphenyl (DCB). DCB was synthesized from 4-bromo-4'-(carbazolyl)biphenyl (BrCB) and diphenylamine using method 1, yielding 0.13 g (27%): ^1H NMR (CDCl_3) δ 8.22 (d, 2H), 7.98 (d, 1H), 7.91–7.18 (m, ca.

21H), 7.12 (t, 2H); MS m/z 486 (M^+ , 100), 408 (2), 319 (7), 243 (M^{2+} , 37), 166 (4), 77 (2); Abs λ_{max} = 295, 340 nm; E_{mm} λ_{max} = 390 nm.

4-Carbazolyl-4'-(phenyl-*m*-tolylamino)biphenyl (TCB). TCB was synthesized from 4-bromo-4'-(carbazolyl)biphenyl (BrCB) and 3-methyldiphenylamine using method 1, yielding 0.35 g (70%): ^1H NMR (CDCl_3) δ 8.15 (d, 2H), 7.78 (d, 2H), 7.59 (d, 2H), 7.55 (d, 2H), 7.50–6.91 (m, ca. 16H), 6.88 (d, 1H), 2.28 (s, 3H); MS m/z 500 (M^+ , 100), 333 (10), 318 (7), 250 (M^{2+} , 62), 166 (12); Abs λ_{max} = 295, 345 nm; E_{mm} λ_{max} = 400 nm.

4-Carbazolyl-4'-(iminodibenzyl)biphenyl (BCB). BCB was synthesized from 4-bromo-4'-(carbazolyl)biphenyl (BrCB) and iminodibenzyl using method 1, yielding 0.27 g (56%): ^1H NMR (CDCl_3) δ 8.14 (d, 2H), 7.76–7.20 (m, ca. 20H), 6.70 (d, 2H), 3.04 (s, 4H); MS m/z 512 (M^+ , 100), 256 (M^{2+} , 19), 194 (11), 167 (5), 152 (6); Abs λ_{max} = 295, 325 nm; E_{mm} λ_{max} = 373 nm. Anal. Calcd for $\text{C}_{40}\text{H}_{32}\text{N}_2$: C, 89.03; H, 5.51; N, 5.46. Found: C, 88.28; H, 5.36; N, 5.33.

4-Carbazolyl-4'-(iminostilbenyl)biphenyl (SCB). SCB was synthesized from 4-bromo-4'-(carbazolyl)biphenyl (BrCB) and iminostilbene using method 1, yielding 0.42 g (73%): ^1H NMR (CDCl_3) δ 8.14 (d, 2H), 7.72–7.22 (m, ca. 20H), 6.87 (s, 2H), 6.41 (d, 2H); MS m/z 510 (M^+ , 100), 343 (11), 332 (10), 315 (13), 255 (M^{2+} , 70), 192 (40), 178 (15), 166 (57), 152 (28), 139 (12); Abs λ_{max} = 295, 315 nm; E_{mm} λ_{max} = 386 nm. Anal. Calcd for $\text{C}_{38}\text{H}_{26}\text{N}_2$: C, 89.38; H, 5.13; N, 5.49. Found: C, 89.27; H, 5.07; N, 5.49.

4-(1-Naphthylphenylamino)-4'-(2-naphthylphenylamino)biphenyl ($\text{N}_\beta\text{N}_\alpha\text{B}$). $\text{N}_\beta\text{N}_\alpha\text{B}$ was synthesized from 4-iodo-4'-(1-naphthylphenylamino)biphenyl (IN_αB) and 2-naphthylphenylamine using method 2, yielding 0.45 g (38%): ^1H NMR (CDCl_3) δ 7.94 (d, 1H), 7.87 (d, 1H), 7.81–6.86 (m, ca. 30H); MS m/z 588 (M^+ , 100), 369 (3), 294 (M^{2+} , 40), 217 (27), 77 (5); Abs λ_{max} = 340 nm; E_{mm} λ_{max} = 431 nm.

4-(1-Naphthylphenylamino)-4'-(diphenylamino)biphenyl (DN_αB). DN_αB was synthesized from 4-iodo-4'-(1-naphthylphenylamino)biphenyl (IN_αB) and diphenylamine using method 2, yielding 0.28 g (43%): ^1H NMR (CDCl_3) δ 7.95 (d, 1H), 7.88 (d, 1H), 7.83–6.85 (m, ca. 28H); MS m/z 538 (M^+ , 100), 369 (3), 269 (M^{2+} , 34), 217 (9), 167 (8), 77 (3); Abs λ_{max} = 310, 350 nm; E_{mm} λ_{max} = 400 (sh), 450 nm.

4-(1-Naphthylphenylamino)-4'-(phenyl-*m*-tolylamino)biphenyl (TN_αB). TN_αB was synthesized from 4-iodo-4'-(1-naphthylphenylamino)biphenyl (IN_αB) and 3-methyldiphenylamine using method 2, yielding 0.24 g (36%): ^1H NMR (CDCl_3) δ 7.93 (d, 1H), 7.86 (d, 1H), 7.81–6.75 (m, ca. 27H), 2.15 (s, 3H); MS m/z 552 (M^+ , 100), 332 (1), 276 (M^{2+} , 25), 217 (7), 167 (5), 77 (3); Abs λ_{max} = 315, 350 nm; E_{mm} λ_{max} = 450 nm.

4-(1-Naphthylphenylamino)-4'-(iminodibenzyl)biphenyl (BN_αB). BN_αB was synthesized from 4-iodo-4'-(1-naphthylphenylamino)biphenyl (IN_αB) and iminodibenzyl using method 2, yielding 0.36 g (32%): ^1H NMR (CDCl_3) δ 7.96 (d, 1H), 7.89 (d, 1H), 7.82 (d, 1H), 7.75 (d, 1H), 7.55–6.82 (m, ca. 21H), 6.59 (d, 1H), 2.99 (s, 4H); MS m/z 564 (M^+ , 100), 369 (5), 344 (3), 282 (M^{2+} , 37), 217 (16), 194 (21), 77 (5). Anal. Calcd for $\text{C}_{42}\text{H}_{32}\text{N}_2$: C, 89.33; H, 5.71; N, 4.96. Found: C, 88.55; H, 5.37; N, 4.55.

4-(1-Naphthylphenylamino)-4'-(iminostilbenyl)biphenyl (SN_αB). SN_αB was synthesized using 4-iodo-4'-(1-naphthylphenylamino)biphenyl (IN_αB) and iminostilbene using method 1, yielding 0.23 g (79%): ^1H NMR (CDCl_3) δ 7.91 (d, 1H), 7.85 (d, 1H), 7.73 (d, 1H), 7.53–6.79 (m, ca. 21H), 6.29 (d, 2H); MS m/z 562 (M^+ , 100), 281 (M^{2+} , 50), 217 (10), 192 (17), 165 (8); Abs λ_{max} = 270, 330 nm; E_{mm} λ_{max} = 404, 507 (br) nm. Anal. Calcd for $\text{C}_{42}\text{H}_{30}\text{N}_2$: C, 89.65; H, 5.37; N, 4.98. Found: C, 87.95; H, 5.32; N, 4.82.

4-(2-Naphthylphenylamino)-4'-(diphenylamino)biphenyl (DN_βB). DN_βB was synthesized from 4-iodo-4'-(2-naphthylphenylamino)biphenyl (IN_βB) and diphenylamine using method 2, yielding 0.37 g (31%): ^1H NMR (CDCl_3) δ 7.81 (t, 2H), 7.67 (d, 1H), 7.58–7.03 (m, ca. 27H); MS m/z 538 (M^+ , 100), 369 (8), 269 (M^{2+} , 58), 217 (23), 167 (12), 77 (9); Abs λ_{max} = 320, 350 nm; E_{mm} λ_{max} = 417 nm.

4-(2-Naphthylphenylamino)-4'-(phenyl-*m*-tolylamino)-biphenyl (TN₂B). TN₂B was synthesized from 4-iodo-4'-(2-naphthylphenylamino)biphenyl (IN₂B) and 3-methyldiphenylamine using method 2, yielding 0.49 g (44%): ¹H NMR (CDCl₃) δ 7.73 (t, 2H), 7.59 (d, 1H), 7.52–6.80 (m, ca. 26H), 2.26 (s, 3H); MS *m/z* 552 (M⁺, 100), 369 (10), 276 (M²⁺, 95), 216 (76), 166 (47), 77 (40); Abs λ_{max} = 320, 350 nm; E_{mm} λ_{max} = 415 nm.

4-(2-Naphthylphenylamino)-4'-(iminodibenzyl)biphenyl (BN₂B). BN₂B was synthesized from 4-iodo-4'-(iminodibenzyl)biphenyl (IBB) and 2-naphthylphenylamine using method 2, yielding 0.27 g (25%): ¹H NMR (CDCl₃) δ 7.76–6.94 (m, ca. 26H), 6.62 (d, 2H), 3.00 (s, 4H); MS *m/z* 564 (M⁺, 100), 368 (15), 296 (15), 282 (M²⁺, 14), 217 (5), 77 (3); Abs λ_{max} = 330 nm; E_{mm} λ_{max} = 414 nm.

4-(2-Naphthylphenylamino)-4'-(iminostilbenyl)biphenyl (SN₂B). SN₂B was synthesized from 4-iodo-4'-(2-naphthylphenylamino)biphenyl (IN₂B) and iminostilbene using method 1, yielding 0.37 g (73%): ¹H NMR (CDCl₃) δ 7.81–6.95 (m, ca. 26H), 6.83 (s, 2H), 6.33 (d, 2H); MS *m/z* 562 (M⁺, 100), 369 (3), 281 (M²⁺, 32), 217 (13), 192 (18), 77 (3); Abs λ_{max} = 280, 330 nm; E_{mm} λ_{max} = 413, 518 (w,br) nm. Anal. Calcd for C₄₂H₃₀N₂: C, 89.65; H, 5.37; N, 4.98. Found: C, 89.54; H, 5.43; N, 4.87.

4-(Diphenylamino)-4'-(phenyl-*m*-tolylamino)biphenyl (TDB). TDB was synthesized from 4-iodo-4'-(diphenylamino)biphenyl (IDB) and 3-methyldiphenylamine using method 1, yielding 0.45 g (80%): ¹H NMR (CDCl₃) δ 7.48–6.80 (m, ca. 27H), 2.25 (s, 3H); MS *m/z* 502 (M⁺, 100), 333 (8), 319 (7), 251 (M²⁺, 68), 167 (15), 77 (8); Abs λ_{max} = 310, 350 nm; E_{mm} λ_{max} = 396 nm.

4-(Diphenylamino)-4'-(iminodibenzyl)biphenyl (BDB). BDB was synthesized from 4-iodo-4'-(diphenylamino)biphenyl (IDB) and iminodibenzyl using method 1, yielding 0.26 g (51%): ¹H NMR (CDCl₃) δ 7.46–6.93 (m, ca. 24H), 6.62 (d, 2H), 3.00 (s, 4H); MS *m/z* 514 (M⁺, 100), 257 (M²⁺, 24), 194 (10), 167 (8), 77 (3); Abs λ_{max} = 340 nm; E_{mm} λ_{max} = 400 nm.

4-(Diphenylamino)-4'-(iminostilbenyl)biphenyl (SDB). SDB was synthesized from 4-bromo-4'-(iminostilbenyl)biphenyl (BrSB) and diphenylamine using method 1, yielding 0.64 g (53%): ¹H NMR (CDCl₃) δ 7.58–6.90 (m, ca. 24H), 6.83 (s, 2H), 6.31 (d, 2H); MS *m/z* 512 (M⁺, 100), 256 (M²⁺, 17), 192 (20), 192 (20), 178 (18), 165 (16), 152 (8), 77 (10); Abs λ_{max} = 310 (sh), 330 nm; E_{mm} λ_{max} = 397, 513 (br) nm.

4-(Phenyl-*m*-tolylamino)-4'-(iminodibenzyl)biphenyl (BTB). BTB was synthesized from 4-iodo-4'-(iminodibenzyl)biphenyl (IBB) and 3-methyldiphenylamine using method 2, yielding 0.28 g (25%): ¹H NMR (CDCl₃) δ 7.45–6.85 (m, ca. 22H), 6.80 (d, 1H), 2.99 (s, 4H), 2.23 (s, 3H); MS *m/z* 528 (M⁺, 67), 348 (17), 194 (66), 179 (74), 178 (100), 151 (38), 77 (32); Abs λ_{max} = 340 nm; E_{mm} λ_{max} = 402 nm.

4-(Phenyl-*m*-tolylamino)-4'-(iminostilbenyl)biphenyl (STB). STB was synthesized from 4-iodo-4'-(iminostilbenyl)biphenyl (ISB) and 3-methyldiphenylamine using method 1, yielding 0.55 g (44%): ¹H NMR (CDCl₃) δ 7.53–6.76 (m, ca. 25H), 6.31 (d, 2H), 2.23 (s, 3H); MS *m/z* 526 (M⁺, 100), 263 (M²⁺, 9), 193 (28), 178 (29), 152 (10), 77 (8); Abs λ_{max} = 310 (sh), 340 nm; E_{mm} λ_{max} = 397, 517 nm.

4-(Iminodibenzyl)-4'-(iminostilbenyl)biphenyl (SBB). SBB was synthesized from 4-iodo-4'-(iminostilbenyl)biphenyl (ISB) and iminodibenzyl using method 1, yielding 0.30 g (48%): ¹H NMR (CDCl₃) δ 7.08–7.56 (m, ca. 20H), 6.82 (s, 2H), 6.57 (d, 2H), 6.29 (d, 2H), 2.98 (s, 4H); MS *m/z* 538 (M⁺, 100), 344 (6), 269 (M²⁺, 32), 194 (16), 192 (20), 178 (13), 165 (12); Abs λ_{max} = 320 nm; E_{mm} λ_{max} = 411, 533 (w,br) nm. Anal. Calcd for C₄₀H₃₀N₂: C, 89.19; H, 5.61; N, 5.20. Found: C, 88.14; H, 5.62; N, 5.10.

Symmetric Phenyls. 1,4-Bis(carbazolyl)benzene (CCP). CCP was synthesized from 1,4-dibromobenzene and carbazole using method 1, yielding g (%): ¹H NMR (CDCl₃) δ 8.18 (d, 4H), 7.81 (s, 4H), 7.57 (d, 4H), 7.47 (t, 4H), 7.33 (t, 4H); MS *m/z* 408 (M⁺, 100), 241 (4), 204 (M²⁺, 50), 166 (8), 140 (8); Abs λ_{max} = 295, 310 nm; E_{mm} λ_{max} = 343 nm.

1,4-Bis(1-naphthylphenylamino)benzene (N₂N₂P). N₂N₂P was synthesized from 1,4-diiodobenzene and 1-naphthylphenylamine using method 2, yielding 15.3 g (26%): ¹H

NMR (CDCl₃); MS *m/z* 512 (M⁺, 100), 293 (10), 256 (M²⁺, 32), 217 (30); Abs λ_{max} = 280, 320 nm; E_{mm} λ_{max} = 505 nm.

1,4-Bis(2-naphthylphenylamino)benzene (N₂N₂P). N₂N₂P was synthesized from 1,4-diiodobenzene and 2-naphthylphenylamine using method 2, yielding 2.15 g (52%): ¹H NMR (CDCl₃) δ; MS *m/z* 512 (M⁺, 100), 369 (5), 293 (15), 256 (M²⁺, 13), 217 (39), 191 (8), 127 (7), 77 (7); Abs λ_{max} = 260, 280, 325 nm; E_{mm} λ_{max} = 471 nm.

1,4-Bis(diphenylamino)benzene (DDP). DDP was synthesized from 1,4-dibromobenzene and diphenylamine using method 1, yielding g (%): ¹H NMR (CDCl₃) δ; MS *m/z* 412 (M⁺, 100), 243 (9), 206 (M²⁺, 9), 167 (44), 77 (30); Abs λ_{max} = nm; E_{mm} λ_{max} = nm.

1,4-Bis(phenyl-*m*-tolylamino)benzene (TTP). TTP was synthesized from 3-iodotoluene and N,N'-diphenyl-1,4-phenylenediamine using method 2, yielding 2.66 g (76%): ¹H NMR (CDCl₃) δ; MS *m/z* 440 (M⁺, 100), 256 (10), 220 (M²⁺, 26), 166 (32), 77 (8); Abs λ_{max} = 315 nm; E_{mm} λ_{max} = 376 nm.

1,4-Bis(iminodibenzyl)benzene (BBP). BBP was synthesized from 1,4-dibromobenzene and iminodibenzyl using method 1, yielding 0.55 g (11%): ¹H NMR (CDCl₃) δ; MS *m/z* 464 (M⁺, 100), 232 (M²⁺, 17), 194 (16), 165 (10); Abs λ_{max} = 315 nm; E_{mm} λ_{max} = 368 nm.

1,4-Bis(iminostilbenyl)benzene (SSP). SSP was synthesized from 1,4-dibromobenzene and iminostilbene using method 1, yielding 1.3 g (47%): ¹H NMR (CDCl₃) δ; MS *m/z* 460 (M⁺, 100), 280 (10), 230 (M²⁺, 13), 192 (11), 165 (8); Abs λ_{max} = 290, 340 nm; E_{mm} λ_{max} = 444, 488 nm.

Symmetric Biphenyls. **1,4-Bis(carbazolyl)biphenyl (CCB).** CCB was synthesized from 4,4'-diiodobiphenyl and carbazole using method 2, yielding 8.25 g (85%): ¹H NMR (CDCl₃) δ 8.16 (d, 4H), 7.91 (d, 4H), 7.70 (d, 4H), 7.57–7.26 (m, 12H); MS *m/z* 484 (M⁺, 100), 315 (7), 242 (M²⁺, 54), 152 (7); Abs λ_{max} = 255, 295, 320 nm; E_{mm} λ_{max} = 389 nm.

1,4-Bis(1-naphthylphenylamino)biphenyl (N₂N₂B). N₂N₂B was synthesized from 4,4'-dibromobiphenyl and 1-naphthylphenylamine using method 1, yielding 13.43 g (67%): ¹H NMR (CDCl₃) δ 7.75 (d 2H), 7.51–6.83 (m 30H); MS *m/z* 588 (M⁺, 100), 294 (M²⁺, 26), 217 (10); Abs λ_{max} = 270, 340 nm; E_{mm} λ_{max} = 450 nm.

1,4-Bis(2-naphthylphenylamino)biphenyl (N₂N₂B). N₂N₂B was synthesized from 4,4'-dibromobiphenyl and 2-naphthylphenylamine using method 1, yielding g (%): ¹H NMR (CDCl₃) δ 7.80 (t, 4H), 7.65 (d, 2H), 7.59–7.17 (m, 24H), 7.11 (t, 2H); MS *m/z* 588 (M⁺, 100), 369 (15), 294 (M²⁺, 84), 217 (33), 242 (19), 191 (20), 115 (10); Abs λ_{max} = 260, 300, 340 nm; E_{mm} λ_{max} = 450 nm.

1,4-Bis(diphenylamino)biphenyl (DDB). DDB was synthesized from 4,4'-dibromobiphenyl and diphenylamine using method 1, yielding 4.14 g (45%): ¹H NMR (CDCl₃) δ; MS *m/z* 488 (M⁺, 100), 319 (6), 244 (M²⁺, 40), 167 (14), 77 (7); Abs λ_{max} = 315 (sh), 355 nm; E_{mm} λ_{max} = 395 nm.

1,4-Bis(phenyl-*m*-tolylamino)biphenyl (TTB). TTB was synthesized from 4,4'-dibromobiphenyl and 3-methyldiphenylamine using method 1, yielding 3.72 g (30%): ¹H NMR (CDCl₃) δ 7.43 (d, 4H), 7.30–6.80 (m, 22H), 2.30 (s, 6H); MS *m/z* 516 (M⁺, 100), 333 (13), 258 (M²⁺, 64), 167 (28), 77 (10); Abs λ_{max} = 315, 355 nm; E_{mm} λ_{max} = 396 nm.

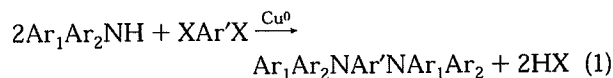
1,4-Bis(iminodibenzyl)biphenyl (BBB). BBB was synthesized from 4,4'-dibromobiphenyl and iminodibenzyl using method 1, yielding 7.8 g (72%): ¹H NMR (CDCl₃) δ; MS *m/z* 540 (M⁺, 100), 270 (M²⁺, 16), 194 (10); Abs λ_{max} = 320 nm; E_{mm} λ_{max} = 402 nm.

1,4-Bis(iminostilbenyl)biphenyl (SSB). SSB was synthesized from 4,4'-dibromobiphenyl and iminostilbene using method 1, yielding 206 g (38%): ¹H NMR (CDCl₃) δ 7.53–7.26 (m, 16H), 7.06 (d, 4H), 6.80 (s, 4H), 6.25 (d, 4H); MS *m/z* 536 (M⁺, 100), 357 (11), 268 (M²⁺, 72), 192 (52), 165 (30); Abs λ_{max} = 300, 340 (sh) nm; E_{mm} λ_{max} = 530 nm.

Results and Discussion

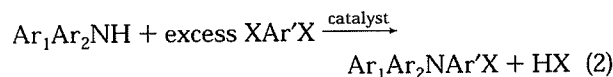
Tetraarylphenylenediamines (e.g., Scheme 1, *n* = 1) and tetraarylbenzidines (e.g., Scheme 1, *n* = 2) have

been extensively investigated as hole transporting materials in xerographic and electroluminescent applications. These materials have the same amine groups bound to either end of the phenylene or biphenylene core. Two materials of this type that are commonly used in electroluminescent applications are TPD and NPD. These are typically prepared by an Ullmann condensation, which involves a copper-catalyzed coupling of an aryl halide and a diarylamine, eq 1. This

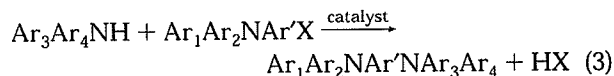


coupling reaction is problematic, producing irreproducible yields and product purities. An alternate synthesis of triarylamines has been developed that utilizes a Pd catalyst²⁵ and reacts under much milder conditions (100 °C for 8–24 h for the Pd-catalyzed reaction vs 190 °C for 2 days for the Ullmann route) to give a significantly purer product. Using both methods, we have prepared a number of symmetric materials for comparison to the asymmetric materials described below. The symmetric compounds fall along the diagonals of Table 1 and Table 2. For a few of these materials (i.e., CCP, CCB), Ullmann coupling reactions reproducibly afford reasonable yields. For most of the materials, however, the Pd-catalyzed coupling reactions are significantly more efficient.

The asymmetric phenylene- and biphenylenediamines reported here have been prepared in two steps. First, a diarylamine is treated with an excess of a dihaloarene (i.e., 1,4-dihalobenzene or 4,4'-dihalobiphenyl), eq 2.



Both Cu- and Pd-catalyzed reactions have been examined for this initial coupling reaction. For Cu-coupling reactions, the dihaloarene used was the diiodo derivative, while for the Pd-catalyzed couplings, the dibromo derivative was used. Excess dihaloarene was used to prevent the coupling of a second equivalent of amine to the dihaloarene. The excess dihaloarene was removed from the product by solvent extraction or sublimation. The singly substituted arene ($\text{Ar}_1\text{Ar}_2\text{NAr}'\text{X}$) was then purified by sublimation. The purified sample of $\text{Ar}_1\text{Ar}_2\text{NAr}'\text{X}$ was then coupled to a second amine, yielding the asymmetric diamine, eq 3, which was subsequently purified by sublimation.



Thermal Properties. It is important for OLEDs to be constructed from materials that are stable glasses to avoid problems associated with grain boundaries in polycrystalline films and to achieve the highest level of uniformity in the vapor-deposited thin films. Many organic molecules can be induced into a glassy state. This occurs when the liquid form of the substance is cooled quickly enough to solidify the sample prior to

crystallization.²⁷ The temperature (or temperature range) where the glass becomes less viscous as it is heated is referred to as the glass transition temperature (T_g). At a temperature above the T_g , the material may crystallize followed by a melting transition at an even higher temperature. It is possible that crystallization may not be observed at all in a given material for kinetic reasons, such that the glass smoothly transforms from a glass to a liquid. Some molecules have greater glass-forming ability than others do. In general, glasses that are stable at high temperatures are formed by asymmetric molecules with reasonably high molecular masses, which have no strong intermolecular forces such as hydrogen bonding. When the liquid sample is cooled rapidly, the molecules are frozen into an amorphous structure. The same amorphous structure is formed on vapor deposition of the materials since the substrate temperature is comparatively cold. Reorganization of this amorphous material to crystalline or polycrystalline material is hindered due to the high energy required to reorient the molecules into the proper crystalline arrangement. If the molecules are symmetric, the amount of molecular reorganization needed to achieve the crystalline structure is low and the material readily crystallizes. Similarly, if the molecules are small, the energy required to reorient the molecules is low and crystallization may occur at a low temperature. The last requirement, listed above for stable glasses (i.e., there are no strong intermolecular forces), is very important. If strong intermolecular forces exist, they may significantly increase the lattice energies helping to drive the material to a crystalline form. In addition, the intermolecular forces can lead to preassociation of the molecules into crystalline aggregates before the melt cools, or while the film is being deposited from vapor. These aggregates can then nucleate crystal growth, preventing the formation of a glass. One of our goals is to understand or draw some general correlations between molecular structure and glass transitions. Foremost though is to improve thermal stability for HTL candidates while retaining their favorable electronic properties.

Most of the asymmetric compounds prepared offer improved thermal stability over TPD; see Tables 1 and 2. As a general trend, the biphenyl derivatives have a higher T_g than the single phenyl derivatives. Compounds such as CCB do not form glasses due to the high level of symmetry and their largely planar structures. Higher T_g s are obtained for materials containing the amines iminostilbene, iminodibenzyl, and/or carbazole. These amines have a hydrocarbon linkage or single bond joining the arene groups, preventing free rotation about the *N*-phenyl bond. Consequently, the ones having two of these three groups incorporated into the molecule have the highest T_g s (SCB, SBB, SSB, and BCB).

A typical DSC for these asymmetric diamines is shown in Figure 2. This plot shows the initial scan of SCB and subsequent heating cycles. Upon first heating no glass transition is observed. This is not surprising since the slow rate of cooling upon sublimation (used to purify the materials) tends to lead to crystalline materials. Once the sample is melted and cooled to room

(27) Murthy, S. S. N.; Gangasharan, Nayak, S. K. *J. Chem. Soc., Faraday Trans.* **1993**, *89*, 509.

Table 1. Thermal, redox, absorption, and Fluorescence Data as Well as the Acronym for Each of the Phenylenediamines Prepared^a

 NAr_2 (column) NAr_2 (row)							
P	C	N _α	N _β	D	T	B	S
	CCP 310/NA 1.041 295,310 343	N_αCP 215/88 0.945 320,350 416	N_βCP 212/83 0.947 285,295,320 409	DCP 158/61 0.965 295,320 400	TCP 139/54 0.950 295,315 370	BCP 233/91 0.958 295 382	SCP 259/103 1.008 270,300 393,487
		N_αN_αP 185/70 0.625 280, 320 505	N_βN_αP NA/81 0.616 280,320 399,496	DN_αP NA/62 0.611 320 414,501	TN_αP NA/60 0.595 320 417,506	BN_αP NA/85 0.551 315 398,510	SN_αP NA/96 0.591 300,350 407
			N_βN_βP 182/68 0.616 260,280,325 471	DN_βP NA/63 0.606 320 399,475	TN_βP NA/59 0.592 320 398,470	BN_βP NA/83 0.569 280,320 398,475	SN_βP NA/96 0.581 280,315 402
				DDP 290/NA 0.602 320,340 394	TDP 169/22 0.593 315 397	BDP 250/56 0.560 310,350 437	SDP NA/66 0.563 310 398
					TTP 175/39 0.561 315 376	BTP NA/54 0.534 320 398	STP NA/70 0.558 315 400
						BBP NA/73 0.416 315 368	SBP 265/109 0.492 310 395
							SSP 304 0.489 290,340 444,488

^a The amine found in the column is bound to the 1 position of the benzene and the amine in the row is bound to the 4 position. The amines found along the diagonal are symmetric (i.e., the same amine is bound to both the 1 and 4 positions), while all of the nondiagonal entries are asymmetric (i.e., they have different amines bound to the 1 and 4 positions). The first line of each entry is the acronym for the given compound. The one-letter designations used for the amines are listed below each amine in the first row. The second line gives the melting point and glass transition (°C), listed mp/*T_g*. For the compounds in which a melting point or *T_g* were not observed the values are denoted NA. The third line is the oxidation potential (V) relative to Ag/AgCl. The fourth line gives the λ_{\max} value(s) (nm) for the solution absorption spectra, and the last line gives the λ_{\max} value(s) (nm) for the solution fluorescence spectra.

temperature, the second heating exhibits a glass transition at 125 °C. If heating is continued beyond the glass transition, a crystallization exotherm is observed. If the scan is stopped before the sample heated above the melt, the subsequent heating cycle will not show a *T_g* or a crystallization exotherm, as expected for a crystalline sample. However, once the sample is melted again and cooled, reemergence of the amorphous phase is seen. This behavior is typical for the asymmetric diamines. Several of the diamines, however, do not crystallize after going through their *T_g*. These molecules may offer

improved lifetime in devices due to their excellent glass-forming ability (i.e., no crystallization over time). These compounds, including SN_αB, STB, BN_αB, and BBB, do not have a well-defined melt.

The asymmetric diamine compounds may also be used to induce glass formation of the symmetric derivatives. For example, CCB shows no glassy form in its DSC, but a sharp melt consistent with a polycrystalline material. Several of the asymmetric diamines have been doped into CCB at varying percentages and found to hinder crystallization. Using this method, a glass transition

Table 2. Thermal, Redox, Absorption, and Fluorescence Data as Well as the Acronym for Each of the Benzidines Prepared^a

 B	 C	 N_α	 N_β	 D	 T	 B	 S
 CCB 290/NA 0.975 255,295,320 389		N_αCB 253/109 1.003 295,330 422	N_βCB 249/107 0.994 295,320,345 404	DCB 217/91 0.975 295,340 390	TCB 198/85 0.925 295,345 400	BCB 273/117 0.992 295,325 373	SCB 291/125 1.040 295,315 386
		NPDB (N_αN_βB) 265/100 0.767 270,340 450	N_βN_αB NA/106 0.775 340 431	DN_αB NA/87 0.779 310,350 400,440	TN_αB NA/85 0.746 315,350 450	BN_αB NA/110 0.709 345 434	SN_αB NA/117 0.772 330 404,507(sh)
			N_βN_βB 265/103 0.794 260,300,340 450	DN_βB NA/92 0.780 320,350 417	TN_βB NA/94 0.750 320,350 415	BN_βB NA/105 0.737 330 414	SN_βB NA/117 0.733 280,330 413,518(sh)
				DDB 236/77 0.751 315,355 395	TDB 184/71 0.766 310,350 396	BDB NA/96 0.7334 340 400	SDB NA/97 0.746 330 397,513(sh)
					TPD (TTB) 175/60 0.733 315,355 396	BTB NA/86 0.702 340 402	STB NA/91 0.720 340 397,517(sh)
						BBB NA/117 0.664 320 402	SBB 295/125 0.691 320 411
							SSB 317/110 0.699 300,340(sh) 530

^a The amine found in the column is bound to the 4 position of the biphenyl and the amine in the row is bound to the 4' position. The amines found along the diagonal are symmetric (i.e., the same amine is bound to both the 4 and 4' positions), while all of the nondiagonal entries are asymmetric (i.e., they have different amines bound to the 4 and 4' positions). The first line of each entry is the acronym for the given compound. The one-letter designations used for the amines are listed below each amine in the first row. The second line gives the melting point and glass transition (°C), listed mp/*T_g*. For the compounds in which a melting point or *T_g* were not observed the values are denoted NA. The third line is the oxidation potential (V) relative to Ag/AgCl. The fourth line gives the λ_{max} value(s) (nm) for the solution absorption spectra, and the last line gives the λ_{max} value(s) (nm) for the solution fluorescence spectra.

for doped CBP of about 107 °C has been observed regardless of which diamine was used as the dopant. The DSC scans shown in Figure 3 illustrate the effect of doping of N_αCP into CCB. The DSC scan shown at the bottom is for pure CBP and shows only a melt transition on the first and all subsequent scans. When CCB and 10% N_αCP are ground together with a mortar and pestle, the DSC scan of the mixture shows two melting transitions on the first heating cycle at 195 and 264 °C, close to the melting temperatures of N_αCP and CCB, respectively. When the sample is then cooled to

room temperature and heated again, a distinct glass transition is observed at 107 °C, a crystallization at 145 °C, and a melt transition at 264 °C. The melting temperature is consistent with that expected for CCB, but a melt for N_αCP is not observed at all. The same thermal behavior is observed for the other dopants that have been examined (N_αCB, TCP, SCP). The level of dopant does not make a significant difference either, with the same thermal behavior being observed for doping levels of 10–50%. At doping levels above 50%, the *T_g* became characteristic of the dopant.

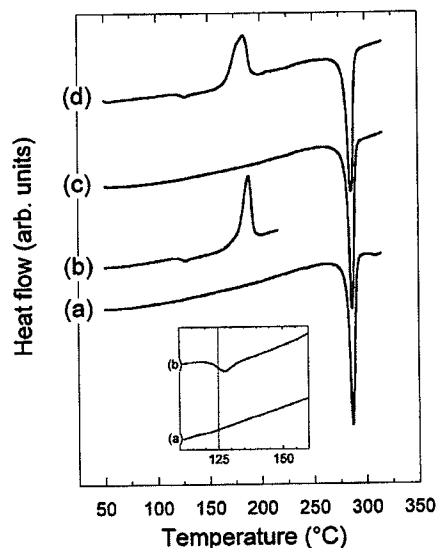


Figure 2. DSC curves for SCB at scan rates of 20 °C/min. (a) The first run shows only crystalline behavior with a melt transition (T_m) at 290 °C. (b) Upon cooling and reheating, the second run displays a glass transition (T_g) at 125 °C along with a crystallization (T_c) at 185 °C. (c) The second run was stopped before the sample was melted; therefore, the third heating cycle only shows crystalline behavior (similar to the first run) with only a melt transition. (d) The fourth heating cycle shows that after the sample has been melted then cooled, it forms a glass with the characteristic T_g . The insert shows expanded scans of (a) and (b) to show the characteristic T_g thermal transition.

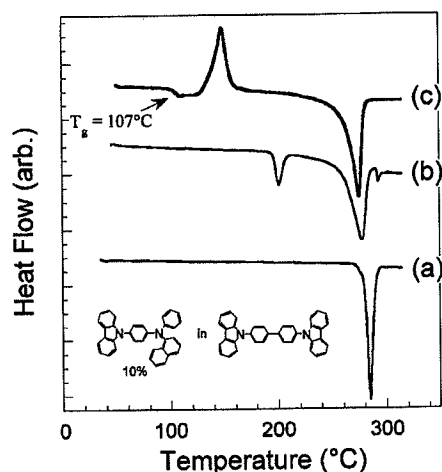


Figure 3. DSC curves (at scan rates of 20 °C/min) for (a) pure CCB. (b) The first run of 10% NaCP doped into CCB shows the characteristic melts of the two compounds with no glass transition. (c) The second run of 10% NaCP doped into CCB shows a glass transition at 107 °C, much higher than that of pure NaCP.

Electrochemistry. In a single heterostructure OLED, holes are carried to the organic interface by the HTL and electrons are carried to the interface by the ETL. For efficient hole/electron recombination, either holes must be injected from the HTL into the ETL or electrons injected into the HTL. To have efficient hole injection from the HTL into the ETL, the energies of the HOMO levels of the two materials must be similar or the HOMO level of the HTL should be below that of the ETL. If the HOMO level of the HTL is above that

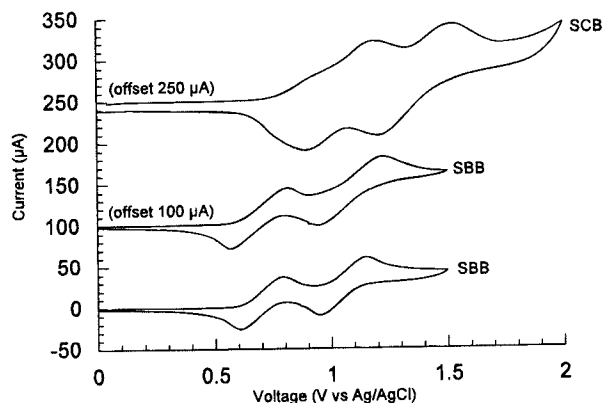


Figure 4. Cyclic voltammograms for iminostilbenyl biphenyl derivatives SCB, SBB, and SSB (see Scheme 1) in CH_2Cl_2 with 0.1 M tetrabutylammonium hexafluorophosphate at scan rates of 0.1 V/s using a Ag/AgCl reference electrode and platinum working and counter electrodes.

of the ETL there will be a barrier to hole injection from the HTL to the ETL. To control the ease of hole injection from the HTL to the ETL it is important to know the relative energies of the HOMO levels of different HTL materials. Estimation of the HOMO energy can be done by a variety of methods, including measuring the ionization potential from films using ultraviolet photoelectron spectroscopy²⁸ and electrochemical measurements. Both methods only lead to estimations of the HOMO energy, since the HOMO energy at the HTL/ETL interface can be significantly altered by charge transfer at the interface.²⁸ In this study, we have chosen to use electrochemical methods to estimate the HOMO energies of the diamine hole transporters.

The electrochemical method used here to measure HOMO energies was cyclic voltammetry (CV). CV scans were recorded from vs Ag/AgCl at a scan rate of 0.1 V/s, with 0.1 M tetrabutylammonium hexafluorophosphate electrolyte in dry, degassed methylene chloride. For our initial experiments, ferrocene was used as an internal reference for calibration.²⁹ We found, however, that the measured oxidation potentials varied as much as 0.15 V from those measurements in the absence of ferrocene. We concluded that there were adverse reactions between our diamines and ferrocene and therefore excluded it from all of the measurements reported here and quote our numbers relative to the Ag/AgCl reference. Each of the diamine compounds exhibits two sequential oxidation processes. The potentials for the first oxidation process of each compound are listed in Tables 1 and 2. The first oxidation process is the one that is expected to be involved in hole transport and transfer to the ETL.

Cyclic voltammetry plots shown in Figure 4 for three compounds in the iminostilbene biphenyl series display three typical curves observed for the diamine compounds. The asymmetric (SBB) and the symmetric (SSB) compounds both exhibit ideal reversible redox

(28) Rajagopal, A.; Kahn, A. *Adv. Mater.* **1998**, *10*, 140 and references therein. Rajagopal, A.; Kahn, A. *J. Appl. Phys.*, in press. Seki, K.; Ito, E.; Ishii, H. *Synth. Met.* **1997**, *91*, 137–142 and references therein.

(29) Gritzner, G.; Kuta, J. *Pure Appl. Chem.* **1984**, *56*, 462.

behavior with two 1-electron oxidation processes followed by symmetric reduction peaks. These observations are representative for all of the diamines prepared excluding those containing carbazole. The oxidation peaks for the carbazole derivatives (e.g., SCB) are quite broad, and there is a larger voltage difference between the oxidation and the reduction waves than seen for the previous examples. These processes are not diffusion limited and are likely irreversible. This is possibly due to instability of the oxidized carbazole species, which results in degradation of the compound in solution.

A number of general trends can be observed in the oxidation potentials listed in Tables 1 and 2. First, all of the compounds (excluding the carbazoles) containing a phenyl bridge have significantly lower oxidation potentials than the corresponding biphenyl derivatives (on average 0.24 V difference). This is easily understood on the basis of the structures of the phenylene and biphenylene groups. Two amine groups can readily communicate through a phenylene group, while the twist between the phenyl groups in the biphenyl linkage effectively breaks conjugation and lessens the interaction between the amine groups. There is also a general trend from low to high oxidation potentials from the derivatives containing iminodibenzyl (B), iminostilbene (S), phenyl-*m*-tolylamine (T), diphenylamine (D), and 1/2-naphthylphenylamine (N_α/N_β) to carbazole (C). This is true for all of the phenyl derivatives (excluding the carbazole derivatives) across each row (or down the columns) and is generally true for most of the biphenyls. This trend can be explained by the relative electron-withdrawing ability of the arenes to the nitrogen. Derivatives with good electron-donating groups on the arenes, such as iminodibenzyl, yield a relatively higher electron density on the nitrogen atoms that in turn allow it to be more easily oxidized. The carbazole derivatives have markedly higher oxidation potentials than all of the others regardless of the amine on the other side. This suggests that the charge of the oxidized species is not localized on one of the nitrogen atoms but is delocalized over the entire molecule.

Although the electrochemical data do not yield exact HOMO levels, we can observe trends and compare the oxidation potentials to well-understood HTL materials with similar structures HTL materials.³⁰ We may be able to explain the observed device characteristics on the basis of the expected HOMO energies and predict what compounds will give the best device performance by supplying the best matches in energy to hole injection and ETL layers.

Electronic Structure. All of the diamines examined here are white or yellow solids. The λ_{max} values for their absorption spectra in CHCl_3 fall between 250 and 350 nm (Tables 1 and 2). The majority of the compounds show small Stokes shifts between the absorption and emission bands (typically 3000–6000 cm^{-1}), leading to violet to blue emission ($\lambda_{\text{max}} = 380\text{--}410\text{ nm}$). We have examined these materials using semiempirical theoretical methods (with the intermediate neglect of differential overlap method, energies and oscillator strength based on CI calculations involving 10 filled and 10

vacant orbitals).³¹ These calculations suggest that for most of the molecules in Table the lowest energy electronic transition is largely due to electron transfer from a nitrogen lone pair to the π^* orbital of the biphenyl group. The calculation predicts that this transition should have a high oscillator strength, consistent with the observed spectra, which have measured extinction coefficients of 10^4 Mcm .

For most of the compounds containing an iminostilbene donor, a moderately low energy band is observed in the emission spectrum at 507–518 nm in addition to the violet/blue emission band. For the symmetric diamine (SSB), the band at 530 nm is the only emission band. For the other iminostilbene-containing molecules, the band above 500 nm is a shoulder and the 380–410 nm band is the strong band. Molecular orbital calculations suggest that the lowest energy electronic transitions in these materials do not involve the biphenyl π system but involve electron transfer from the amine nitrogen to the π^* system of the stilbene. A nitrogen to biphenyl π^* transition is also present in the asymmetric materials, at higher energies, with significantly higher oscillator strengths. There are several possible explanations for the large Stokes shift in SSB. Emission from an SSB excimer would lead to significantly red-shifted emission; however, dilution studies show the same emission spectrum at high levels of dilution, precluding excimer or aggregate state emission. If the molecule crosses over to a triplet excited state that could also lead to a significant red shift in emission. The photoluminescent lifetimes for these materials are not consistent with triplet emission. The lifetime for SSB in CHCl_3 solution is 6 ns, consistent with singlet emission. The asymmetric iminostilbene biphenyl derivatives (SCB, SN_αB , SN_βB , SDB, STB, SBB) have emission lifetimes for the blue/violet band (380–410 nm) ranging from 1.5 to 3 ns and lifetimes for the green band of 5.5–6.5 ns. The lifetimes for the violet/blue band in these asymmetric derivatives are consistent with the other diamines, whose transitions are associated with nitrogen to biphenyl π^* transitions. The green band only occurs in the iminostilbene derivatives and is most likely due to transition within the iminostilbene group. The large Stokes shift in these materials is not due to excimer or triplet states. A logical proposal for the origin of the large Stokes shift in these materials is that the intense absorption in the ultraviolet is not related to iminostilbene emission. The absorption band for the iminostilbene moiety would be close to 500 nm and may be overshadowed by the intense N to biphenyl π^* band. The excitation spectra of the iminostilbene materials support this conclusion. The excitation spectra of the iminostilbene compounds show an intense band below 400 nm, as expected based on the absorption spectra, and a weak band centered between 450 and 500 nm.

Conclusions

This systematic study of triaryldiamines has supplied some very practical information as to what types of

(30) Katsuma, K.; Shirota, Y. *Adv. Mater.* **1998**, *10*, 223. Thelakkat, M.; Schmidt, H.-W. *Adv. Mater.* **1998**, *10*, 219.

(31) Anderson, W. P.; Edwards, W. D.; Zerner, M. C. *Inorg. Chem.* **1986**, *25*, 2728. Anderson, W. P.; Cundari, T. R.; Drago, R. S.; Zerner, M. C. *Inorg. Chem.* **1990**, *29*, 1. Kotzian, M.; Rosch, N.; Schroeder, H.; Zerner, M. C. *J. Am. Chem. Soc.* **1989**, *111*, 7687. ZINDO was run on a Silicon Graphics, Indigo-2 workstation, using Biosym International software.

materials should perform well as HTLs in OLEDs. By varying the arylamines, we have shown which amines in general yield the best thermal stability. The iminostilbene and iminodibenzyl derivatives consistently give higher T_g values than any of the other amines. Electrochemical and spectroscopic measurements give a good picture of the relative HOMO levels and energy gaps for these materials, which are important parameters in the design of efficient OLEDs. In this way, an HTL can be tailored to suit the device application. The asymmetric compounds show enhanced thermal stability over those of the symmetric derivatives due to their ability to form stable glasses and preventing crystallization. For many of these compounds, these thermal enhancements have not hindered but have improved the

desired properties exhibited by TPD. We are currently investigating the transport properties of these materials and their use as HTLs in OLEDs.

Acknowledgment. The authors would like to thank the Universal Display Corporation, the Defense Advanced Research Project Agency, and the National Science Foundation for their financial support of this work.

Supporting Information Available: Photoluminescence spectra and lifetimes for SSB, SCB, SN_aB , SN_pB SDB, STB, SBB, as described in the text (2 pages). Ordering information is given on any current masthead page.

CM980186P

Comparison of Charge-Carrier Transport in Thin Films of Spiro-Linked Compounds and Their Corresponding Parent Compounds**

By Tobat P. I. Saragi, Thomas Fuhrmann-Lieker, and Josef Salbeck*

The charge-transport properties of the spiro-linked compounds 2,2',7,7'-tetrakis(diphenylamino)-9,9'-spirobifluorene, 2,2',7,7'-tetrakis(*N,N'*-di-*p*-methylphenylamino)-9,9'-spirobifluorene, 2,2',7,7'-tetra(*m*-tolyl-phenylamino)-9,9'-spirobifluorene, and 2,2',7,7'-tetra(*N*-phenyl-1-naphthylamine)-9,9'-spirobifluorene, and their corresponding parent compounds, *N,N,N',N'*-tetraphenylbenzidine, *N,N,N',N'*-tetrakis(4-methylphenyl)benzidine, and *N,N'*-bis(3-methylphenyl)-(1,1'-biphenyl)-4,4'-diamine, *N,N'*-diphenyl-*N,N'*-bis(1-naphthyl)-1,1'-biphenyl-4,4'-diamine, are investigated. The field-effect mobilities of charge carriers in thin films of the parent compounds are slightly higher than those of the spiro-linked compounds. However, the transistor action of the parent-compound thin films vanishes because the films crystallize after being stored in ambient atmosphere for a few days. In contrast, the hole mobilities in thin films of the spiro-linked compounds do not change significantly after the samples are stored in ambient atmosphere for up to nine months. Also discussed is the temperature dependency of the mobilities of charge carriers, which is presented using two models, namely the Arrhenius and the Gaussian disorder models.

1. Introduction

Organic semiconductors are of interest for manufacturing large-area and flexible organic electronic devices at very low cost. The reliability of organic electronic devices depends on the morphological stability of the corresponding materials, which can be quantified by the glass-transition temperature (T_g) of the materials. One important class of functional materials employed in organic light-emitting devices (OLEDs)^[1,2] and in organic field-effect transistors (OFETs)^[3] are hole-transport materials. One well-known example is *N,N'*-diphenyl-*N,N'*-bis(1-naphthyl)-1,1'-biphenyl-4,4'-diamine (α -NPB), which has a T_g of 95 °C and an ionization potential of 5.1 eV.^[1] However, the T_g of α -NPB is not high enough to prevent thin films of the material from crystallizing.

In 1996, Salbeck^[4] introduced the spiro concept in order to improve the morphological stability of functional organic glasses while retaining their functionality.^[4–7] Joining two charge-transport moieties (for instance, two identical α -NPB molecules) through a spiro-carbon center has the effect of raising the T_g , because the increased steric demand of the resulting spiro-linked compound, 2,2',7,7'-tetra(*N*-phenyl-1-naphthyl-

amine)-9,9'-spirobifluorene (spiro- α -NPB), effectively hinders crystallization. The T_g of the resulting spiro- α -NPB is 147 °C. The perpendicular arrangement of the two α -NPB moieties in spiro- α -NPB is expected to give only relatively weak electronic interaction between the molecular halves. Generally, spiro-linked compounds are known to be glass-forming materials with high T_g and good morphological stability, which makes them well-suited for organic devices. Spiro-linked compounds have been successfully applied in organic solar cells,^[6] OLEDs,^[6–8] OFETs,^[9,10] phototransistors,^[11] and lasers.^[12–14]

However, the influence of the spiro center on the electrical properties of the spiro-linked compound in comparison with the corresponding parent compound requires further investigation. In this paper, a comparison between the hole-transport properties in thin films of spiro-linked triarylamine compounds and their corresponding parent compounds are undertaken. The materials used in this study are shown in Figure 1: 2,2',7,7'-tetrakis(diphenylamino)-9,9'-spirobifluorene (spiro-TAD), 2,2',7,7'-tetrakis(*N,N'*-di-*p*-methylphenylamino)-9,9'-spirobifluorene (spiro-TTB), 2,2',7,7'-tetra(*m*-tolyl-phenylamino)-9,9'-spirobifluorene (spiro-TPD), 2,2',7,7'-tetra(*N*-phenyl-1-naphthylamine)-9,9'-spirobifluorene (spiro- α -NPB), *N,N,N',N'*-tetraphenylbenzidine (TAD), *N,N,N',N'*-tetrakis(4-methylphenyl)benzidine (TTB), *N,N'*-bis(3-methylphenyl)-(1,1'-biphenyl)-4,4'-diamine (TPD), and *N,N'*-diphenyl-*N,N'*-bis(1-naphthyl)-1,1'-biphenyl-4,4'-diamine (α -NPB). The field-effect transistor (FET) method has been used in our experiment for extracting physical parameters such as the field-effect mobility of charge carriers. Table 1 summarizes the first oxidation potentials, obtained from electrochemical measurements in CH_2Cl_2 , and the calorimetric T_g values of the active materials used in this study. Figure 2 shows the schematic view of a bottom-contact OFET and the chemical structures of the parent compounds and their corresponding spiro-linked compounds.

[*] Prof. J. Salbeck, Dr. T. P. I. Saragi, Dr. T. Fuhrmann-Lieker
Macromolecular Chemistry and Molecular Materials (mmCmm)
Department of Sciences and Center for Interdisciplinary
Nanostructure Science and Technology (CINsaT)
University of Kassel
Heinrich-Plett-strasse 40, 34109 Kassel (Germany)
E-mail: salbeck@uni-kassel.de

[**] The DAAD fellowship is gratefully acknowledged to support one of the authors (T. P. I. S.). We also thank T. Spehr for a critical reading of the manuscript.

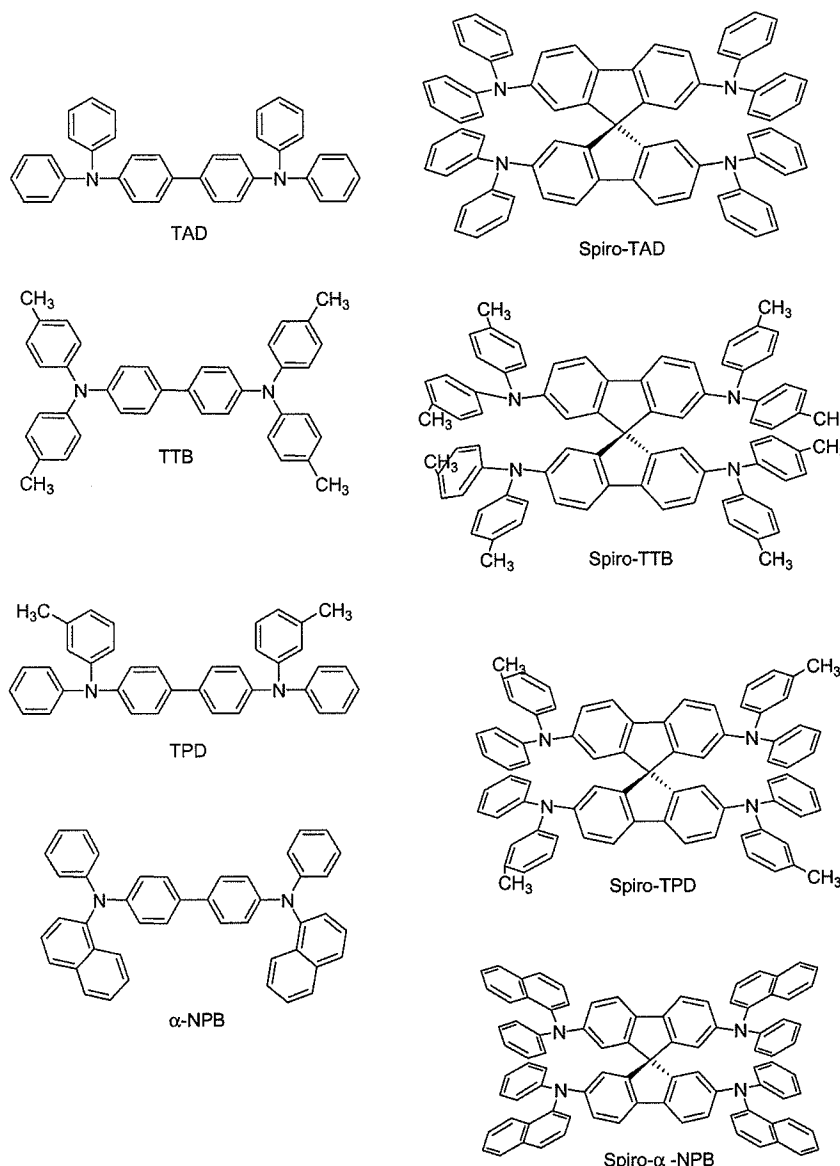


Figure 1. The chemical structures of materials used in this study.

Table 1. The first oxidation potential and the glass-transition temperature of the materials used in this study.

Material	E_{ox} versus Fc/Fc^+ [V]	T_g [°C]	Ref.
TAD	0.290	70	[15]
Spiro-TAD	0.203	133	[15,16]
TPD	0.266	62	[15,17]
Spiro-TPD	0.168	115	[15,16]
TTB	0.183	66	[15]
Spiro-TTB	0.075	146	[15,16]
α-NPB	0.295	95	[4,15]
Spiro α-NPB	0.202	147	[15,16]

2. Results and Discussion

2.1. Electrical Characteristics of and Morphological Changes in Parent-Compound Thin Films

The output and transfer characteristics of an α-NPB FET measured in air and vacuum are shown in Figure 3. Figure 3a shows the output characteristics of an α-NPB FET measured in air and under vacuum. The drain current increases as the gate voltage is increased towards a larger negative voltage, exhibiting an effective field-effect modulation, caused by the gate bias. The sign of the field-enhanced current, I_D , ($I_D < 0$ with $V_G < 0$, where V_G is the gate bias) is consistent with an accumulation regime, owing to the p-type character of α-NPB. At low drain bias, the characteristics exhibit some nonlinearities that can be attributed to the non-ohmic contact between α-NPB and the gold electrodes. This general behavior was found in all transistors based on thin films of the parent compounds and their corresponding spiro-linked compounds. The saturated drain current measured in air (at $V_D = V_G = -60$ V, where V_D is the drain bias) was $0.49 \mu A$, and this increased by 53 % when measured under vacuum. The measurements performed under vacuum were carried out after the sample was stored in a continuously evacuated chamber for 24 h.

An ON/OFF ratio of 2.5×10^5 ($V_D = -60$ V) was obtained for operation in air as the gate bias was scanned from 0 to -60 V. In the saturation regime, a mobility value of $4.1 \times 10^{-5} \text{ cm}^2 \text{ V}^{-1} \text{ s}^{-1}$ and a fitted threshold voltage of -6.7 V were obtained. However, the device turned on at -4 V. Figure 3b clearly shows that the drain current of a α-NPB FET in the OFF state is higher under vacuum ($I_{OFF} \approx 0.2 \text{ nA}$) than in air ($I_{OFF} \approx 2 \text{ pA}$). As a result, the measurements performed under vacuum gave an ON/OFF

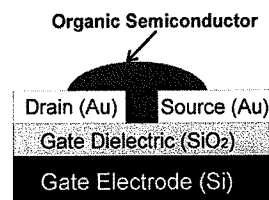


Figure 2. A schematic view of a bottom-contact organic FET.

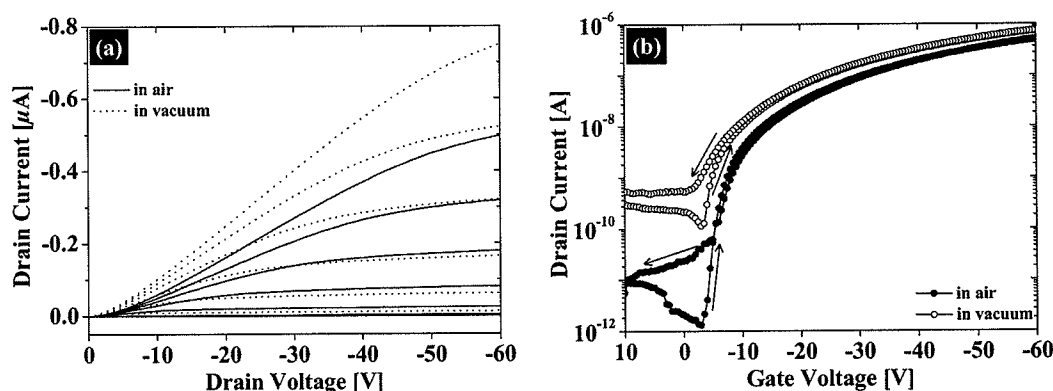


Figure 3. Output and transfer characteristics of an α -NPB FET ($W=2$ mm, $L=5$ μ m, $C_i=17.3$ nF cm $^{-2}$). a) Output characteristics measured in air and under vacuum. The gate bias was swept from +10 to -60 V in steps of 10 V. b) Transfer characteristics measured in air and under vacuum ($V_D=-60$ V). The arrows show the direction of the gate bias being swept during measurement. W , L , C_i , and V_D denote the channel width, the channel length, the capacitance of the gate dielectric per unit area, and the drain bias, respectively.

ratio of 3.5×10^3 ($V_D=-60$ V) as the gate bias was scanned from 0 to -60 V, which is a lower ratio than the value obtained from the measurement performed in air. The hole mobility and the threshold voltage measured under vacuum were 6.1×10^{-5} cm 2 V $^{-1}$ s $^{-1}$ and -4.4 V, respectively. We also observed a small hysteresis in the transfer characteristics at low gate biases. After the sample was placed in a continuously evacuated chamber for more than 30 h, field effects were no longer observed. This result implies that even when a sample is stored in a continuously evacuated chamber for 24 h, the aging of the thin films cannot be inhibited. Moreover, it seems that the aging of the device begins immediately after the deposition of α -NPB.

In order to investigate the aging of the device, we measured the surface morphology of α -NPB twice. First, an atomic force microscopy (AFM) image was recorded after the deposition of α -NPB. Then, the second image was recorded after the sample was stored in ambient atmosphere, in the dark, and at room temperature (RT) for a few days.

Figure 4a shows that the surface of as-deposited α -NPB thin films is relatively smooth and flat with a mean roughness of 0.43 nm and a peak-to-valley height of 2.86 nm. However, after the sample was stored in an ambient atmosphere, in the dark, and at RT for three days, the α -NPB films underwent a distinctive change in the surface morphology in which the mean surface roughness increased significantly. As shown in Figure 4b, the film morphology undergoes a transition from a homogeneous surface to a worm-like structure with sharp edges separated by large voids. The mean roughness has increased by a factor of 84 and the peak-to-valley height is 187 nm. This indicates that α -NPB thin films crystallize easily when the samples are left in an ambient atmosphere for three days. We have also observed the surface morphology of films grown on a p-Si substrate, a SiO $_2$ /p-Si substrate, and a glass substrate by using optical microscopy, and found that these films

also crystallize easily.^[15] Therefore, the disappearance of the transistor action of an α -NPB FET after being stored for a few days in an ambient atmosphere is most probably caused by the change in the film morphology.

As a second example, Figure 5 shows the time dependency of the saturated drain current (at $V_D=V_G=-60$ V) and field-effect mobility of charge carriers in thin films of TAD. Initially, the saturated drain current increases substantially when the device is stored for 24 h in a continuously evacuated chamber. However, the saturated drain current decreases by 47 % after the chamber is continuously evacuated for a further 51 h (total storage time, 75 h). Finally, the saturated drain current reaches nearly zero after the device is stored under vacuum for a total of more than 150 h, and no transistor effect is observed. This implies that device aging takes place even if the sample is placed or stored in a dynamic vacuum. The AFM and optical microscopy images of TAD thin films on various substrates support this result that TAD thin films crystallize easily after the samples are stored in ambient atmosphere at RT for a few days.^[15]

Table 2 displays the charge-carrier mobilities in thin films of parent compounds extracted from time-of-flight (TOF), transient electroluminescence (TEL), and FET techniques. Generally, two main factors influence the hole mobility in the amorphous thin films investigated in this study: the first oxidation potential, which determines the effectivity of the charge injection.

Table 2. Hole mobilities in thin films of parent compounds measured at room temperature.

Material	Method	Hole mobility [cm 2 V $^{-1}$ s $^{-1}$]	Ref.	Material	Method	Hole mobility [cm 2 V $^{-1}$ s $^{-1}$]	Ref.
TAD	FET	$(6.7 \pm 0.5) \times 10^{-5}$	this work	TTB	TOF	7×10^{-4}	[18]
TPD	FET	$(8.7 \pm 0.5) \times 10^{-5}$	this work	TTB	TOF	1×10^{-3}	[21]
TTB	FET	$(1.8 \pm 0.6) \times 10^{-5}$	this work	α -NPB	FET	4.58×10^{-5}	[22]
α -NPB	FET	$(6.1 \pm 0.5) \times 10^{-5}$	this work	α -NPB	TOF	5.1×10^{-4}	[23]
TPD	TOF	1×10^{-3}	[18]	α -NPB	FET	9.3×10^{-8}	[24]
TPD	TOF	1×10^{-3}	[19]	α -NPB	TEL	$(1-3) \times 10^{-4}$	[25]
TPD	TOF	$(2-3) \times 10^{-3}$	[20]				

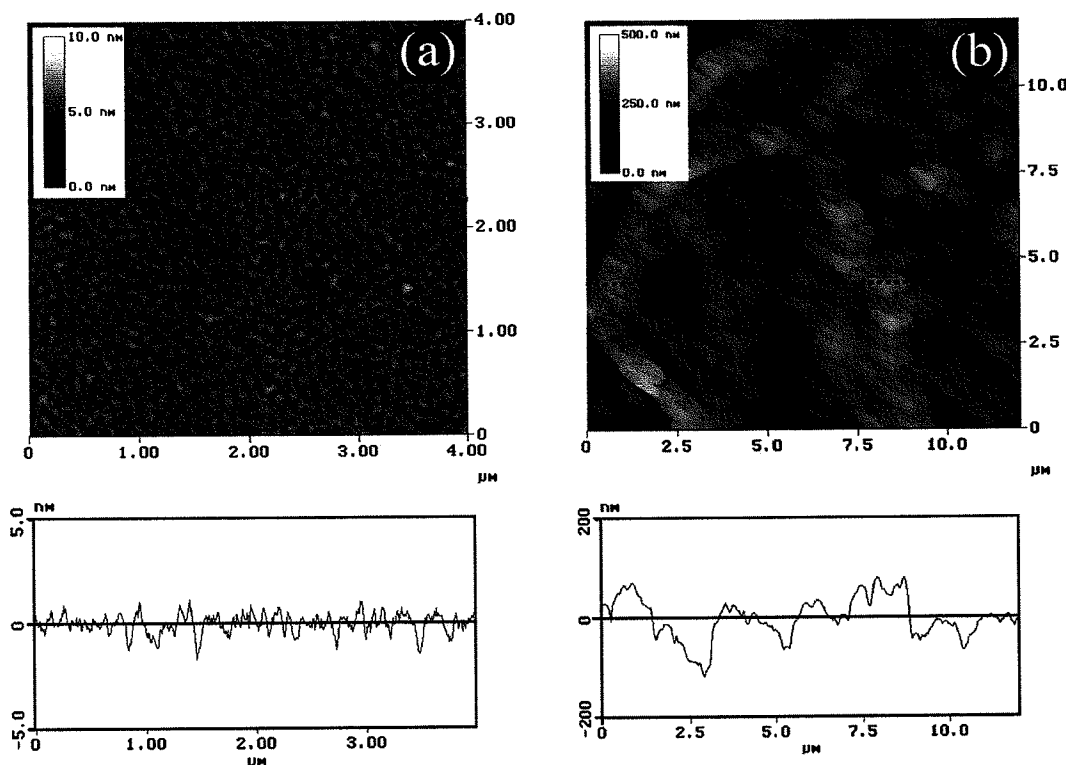


Figure 4. AFM topographical images of an α -NPB thin film on $\text{SiO}_2/\text{p-Si}$, as-deposited (a), and after the sample was stored in ambient atmosphere, in the dark, and at RT for three days (b). The analysis of the cross section describes the peak-to-valley height of a selected line on the AFM image. The selected lines are denoted by dotted lines across the images.

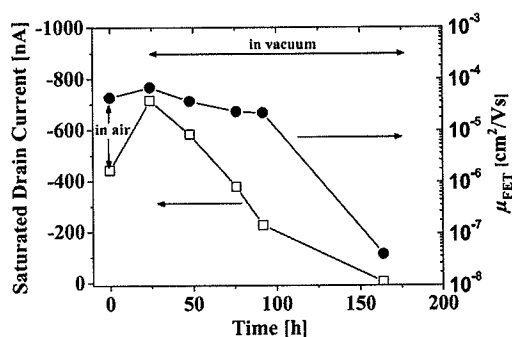


Figure 5. Drain current of a TAD FET measured first in air and then in a continuously evacuated chamber. The saturated drain current was measured at $V_D = V_G = -60$ V. The saturated drain current is plotted linearly versus time (left side) and the field-effect mobility is plotted semi-logarithmically versus time (right side).

tion between the electrodes and the active materials during device operation, and the morphological stability. We have found that the hole mobility in thin films of TTB is the lowest among the parent compounds. This value can be correlated to the relatively low value of the first oxidation potential of TTB compared with the other parent compounds, as shown in Table 1. As a consequence, the potential barrier for charge injection between the electrode and TTB is the largest among the parent

compounds and, thus, the lowest hole mobility is obtained. On the other hand, the first oxidation potentials of TAD, TPD, and α -NPB are roughly the same. Another aspect is the T_g of the corresponding compounds. All parent compounds have T_g values lower than 100°C . Thus, all films crystallize easily after the samples are left in an ambient atmosphere for a few days, resulting in a reduced mobility. For TPD, the charge-carrier mobility decreased by a factor of eight after the sample was left in an ambient atmosphere for seven months.

Generally, the values obtained by using the FET technique are one to two orders of magnitude lower than the values obtained from the TOF technique. von Malm has reported the field-effect mobility of holes in an α -NPB thin film utilizing a bottom-contact organic FET to be $4.58 \times 10^{-5} \text{ cm}^2 \text{ V}^{-1} \text{ s}^{-1}$ ($W = 20 \text{ cm}$, $L = 5 \text{ }\mu\text{m}$, $C_i = 15 \text{ nF cm}^{-2}$, where W , L , and C_i denote the channel width, the channel length, and the capacitance of the gate dielectric per unit area, respectively).^[22] This result agrees very well with ours.

The mobilities of charge carriers in thin films of α -NPB have also been reported by other groups. Chen et. al have measured the hole mobility in $1 \text{ }\mu\text{m}$ thick films of α -NPB at an electric field of 10^5 V cm^{-1} by utilizing the TOF method.^[23] They reported a mobility of $5.1 \times 10^{-4} \text{ cm}^2 \text{ V}^{-1} \text{ s}^{-1}$. Iizuka et al. have reported the field-effect mobility of holes in α -NPB thin films using a bottom-contact FET ($W = 116 \text{ mm}$, $L = 100 \text{ }\mu\text{m}$, $C_i = 17.3 \text{ nF cm}^{-2}$). The temperature of the substrate during the

thermal deposition process was kept constant at 80 °C.^[24] A hole mobility of $9.3 \times 10^{-8} \text{ cm}^2 \text{ V}^{-1} \text{ s}^{-1}$ was reported. This value is different from the values obtained in our experiment. The difference in mobility values can probably be attributed to different substrate temperatures, pretreatment of the substrates, or thermal evaporation parameters. Kovac et al. utilized TEL measurements to extract the hole mobility in α -NPB thin films.^[25] They found a mobility of $(1-3) \times 10^{-4} \text{ cm}^2 \text{ V}^{-1} \text{ s}^{-1}$, which is similar to the values obtained using the TOF technique.

2.2. Electrical Characteristics of Spiro-Linked-Compound Thin Films

Figure 6 shows the output and transfer characteristics of a spiro- α -NPB FET, for a fresh sample measured in air and under vacuum. At low drain biases, a nonlinear behavior of the drain current versus drain bias is observed, as shown in Figure 6a, which could be attributed to the non-ohmic contacts between the gold electrodes and spiro- α -NPB. The field-effect mobility of holes measured upon exposure to air was $2.9 \times 10^{-5} \text{ cm}^2 \text{ V}^{-1} \text{ s}^{-1}$. The fitted threshold voltage was -4.2 V . In contrast, the switch-on voltage of the device measured in air was 0 V , as

shown in Figure 6b. Moreover, an ON/OFF ratio of typically 1.8×10^5 for $V_D = -60 \text{ V}$ can be obtained from the transfer characteristics when the gate bias is scanned from 0 to -60 V .

Figure 6a also shows the output and transfer characteristics measured under vacuum. The saturated drain current (at $V_D = V_G = -60 \text{ V}$) measured under vacuum was 30 % higher than the values measured in air. The fitted threshold voltage was -4.2 V , which is the same as the value obtained from the measurement carried out in air. The field-effect mobility of holes was $4.3 \times 10^{-5} \text{ cm}^2 \text{ V}^{-1} \text{ s}^{-1}$. This value is slightly higher than that obtained from the measurement carried out in air. However, the hole mobility (measured in air and under vacuum) in thin films of spiro- α -NPB is slightly lower than that of α -NPB. Comparing the measurements performed in air and under vacuum, the ON/OFF ratios of devices measured under vacuum increased to 2.6×10^5 for $V_D = -60 \text{ V}$ as the gate bias was swept from 0 V to -60 V . Moreover, the device did not show any significant hysteresis in the transfer characteristics for measurements carried out either in air or under vacuum. This implies that spiro- α -NPB FETs are stable under operation in ambient atmosphere. We have also compared the hole mobilities in thin films of spiro-TAD, spiro-TTB, and spiro-TPD with the corresponding parent compounds. Generally, the hole mobilities in fresh thin films of the parent compounds are slightly higher than those in spiro-linked compounds (Tables 2 and 3). However, the thin-film transistors based on spiro-linked compounds are more stable under operation in air compared with their corresponding parent compounds. The same device was then stored at RT, in the dark, and in ambient atmosphere

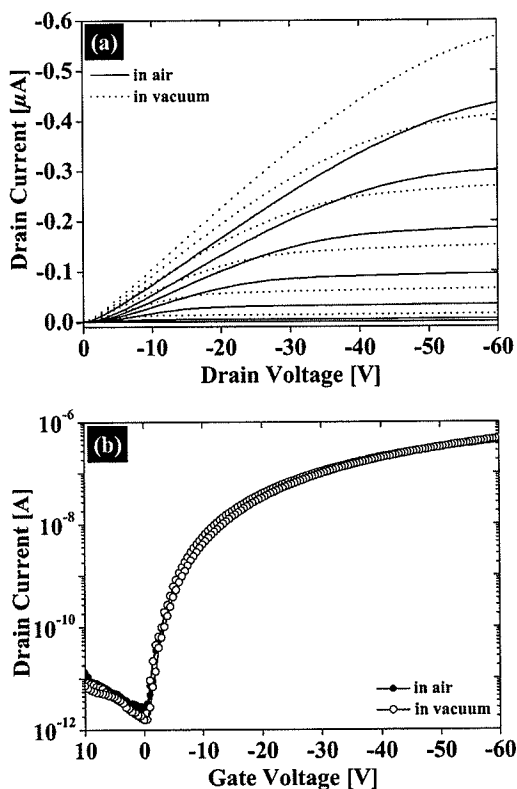


Figure 6. Output and transfer characteristics of a spiro- α -NPB FET ($W = 5 \text{ mm}$, $L = 10 \text{ }\mu\text{m}$, $C_i = 19.9 \text{ nF cm}^{-2}$). a) Output characteristics measured in air and under vacuum. The gate bias was swept from $+10$ to -60 V in steps of 10 V . b) Transfer characteristics measured in air and under vacuum ($V_D = -60 \text{ V}$).

Table 3. Hole mobilities in thin films of spiro-linked compounds extracted from FET measurements.

Material	Hole mobility at RT [$\times 10^{-5} \text{ cm}^2 \text{ V}^{-1} \text{ s}^{-1}$]	Stability	Ref.
Spiro-TAD	6.7 ± 0.3	Stable in air up to 9 months, mobility decreased by 2 %	[10]
Spiro-TPD	6.9 ± 0.4	Stable in air up to 9 months, mobility decreased by 3 %	[10]
Spiro-TTB	5.7 ± 0.5	Stable in air up to 4 months, mobility decreased by 13 %	this work
Spiro- α -NPB	4.4 ± 0.2	Stable in air up to 3 months, mobility decreased by 4 %	this work

for three months. After that, the transistor characteristics were measured again. The results are shown in Figure 7. We have found that after three months the saturated drain current (at $V_D = V_G = -60 \text{ V}$ and measured under vacuum) decreased by 11 % and the hole mobility decreased by only 4 %. However, the switch-on voltage of the transistor, V_{so} , which was 0 V for a fresh device, has slightly shifted toward positive bias after 3 months ($V_{so} \approx +1 \text{ V}$). A similar result was also obtained for the fitted threshold voltage, which shifts from -4.2 to -4.8 V for in-air operation, after the sample was stored for 3 months. Moreover, an ON/OFF ratio of 2×10^5 for $V_D = -60 \text{ V}$ was obtained as the gate bias was scanned from $+1$ to -60 V when

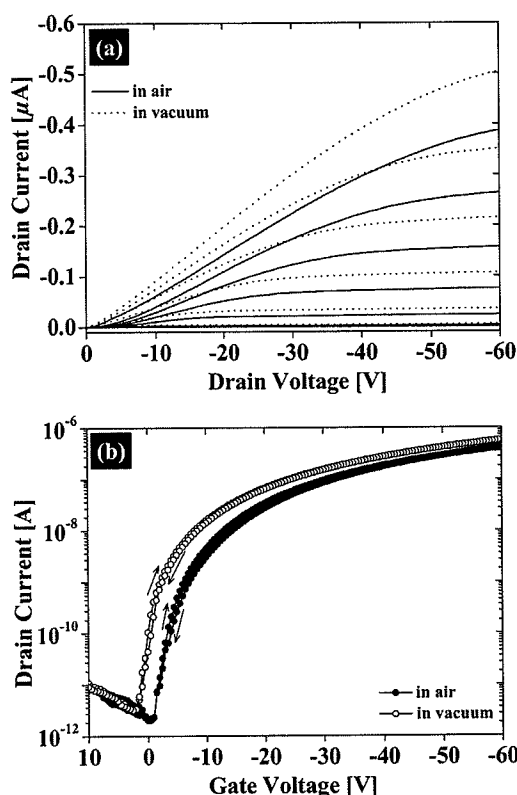


Figure 7. Output and transfer characteristics of a spiro- α -NPB FET, measured after the sample has been stored in ambient atmosphere for 3 months ($W=5$ mm, $L=10$ μ m, $C_i=19.9$ nFcm $^{-2}$). a) Output characteristics measured in air and under vacuum. The gate bias was swept from +10 V to -60 V in steps of 10 V. b) Transfer characteristics measured in air and under vacuum ($V_D=-60$ V). The arrows show the direction of the gate bias being scanned during the measurement.

measured in air. The measurement carried out under vacuum gave an ON/OFF ratio of 1.9×10^5 for $V_D=-60$ V as the gate bias was scanned from +2 to -60 V, which is only slightly lower than the values measured for a fresh device. We have also observed a hysteresis in the transfer characteristics after the sample was stored in ambient atmosphere for 3 months. Probably, this hysteresis is due to the presence of trapped mobile charges that came from moisture as the sample was stored in ambient atmosphere. As also reported previously, the morphology of symmetrically spiro-linked compounds did not change significantly when the samples were left in an ambient atmosphere for nine months.^[9] Table 3 summarizes the FET hole mobilities obtained for the spiro-linked compounds. The hole mobility of spiro- α -NPB is the lowest among the investigated compounds. Also, we have observed that spiro-TTB is relatively unstable against aging, compared with the other spiro-linked compounds.

As mentioned in the earlier part of Section 2.1., the output characteristics of all transistors based on parent compounds and their corresponding spiro-linked compounds exhibit a non-linear behavior at low drain bias. The non-ohmic hole injection is expected, because the highest occupied molecular orbital of

the active compounds does not exactly match the work function of the gold electrodes. Therefore, there is a potential barrier for charge injection to the active compounds and the gold electrode does not make ohmic contact with the active compounds. Consequently, organic transistors based on spiro-linked compounds and their corresponding parent compounds suffer from large contact resistance. This effect means that the estimation of the charge-carrier mobility is not optimal. This issue is still a major challenge in organic-transistor research. Our experimental data also show that the hole mobilities calculated in the linear regime (for instance at $V_D=-5$ V) are $(0.43 \pm 0.03) \times 10^{-5}$ and $(0.35 \pm 0.02) \times 10^{-5}$ cm 2 V $^{-1}$ s $^{-1}$ for α -NPB and spiro- α -NPB, respectively. Those values are approximately one order of magnitude lower than those obtained in the saturation regime. We have found that the computed linear mobilities are always lower than the calculated saturation mobilities for all the transistors presented in this paper. The behavior in the linear regime is more strongly affected by the interface properties and contacts than in the saturation regime. Any bias drop across the electrode/active compound interfaces will lower the effective bias across the channel. Therefore, the apparent currents that are used to compute the mobility are underestimated. However, in the saturation regime the bias drop has a small effect, since the current is relatively independent of the drain bias.

2.3. Temperature Dependence

A few models have been proposed to explain the temperature dependence of the mobility of charge carriers in amorphous organic conjugated materials; these include the Arrhenius model^[26] and the Gaussian disorder formalism.^[27,28] The first, the Arrhenius model, describes the hopping transport as resulting from a single level of traps or an activation energy arising from polaron relaxation.^[26] This model predicts that the mobility of charge carriers is proportional to the reciprocal of the temperature ($\ln \mu \sim 1/T$). The second, the Gaussian disorder (GD) model or Bässler model, uses the notion that both the energy levels and intersite distances of the transport sites are subject to a distribution function in an amorphous solid. The authors assume a Gaussian distribution for both the energetic and the positional disorder, supported by the fact that the absorption profiles of amorphous materials generally feature Gaussian line shapes. Monte Carlo simulation methods are based on the Miller–Abrahams jump rates of hopping processes from within a Gaussian distribution of localized states.^[27,28] As a result, the charge-carrier mobility is predicted to be proportional to the inverse square of the temperature ($\ln \mu \sim 1/T^2$).

Figure 8 shows the field-effect mobilities of charge carriers in thin films of TPD and spiro-TPD as a function of temperature. The dependency of the field-effect mobility on the temperature is shown in two ways, in a plot of the field-effect mobility versus the reciprocal of the temperature in the Arrhenius representation and in a plot of the field-effect mobility versus the inverse square of the temperature in the GD model. We have found that the Arrhenius model fits our experimental data better than the GD model.^[15] Prefactor mobilities μ_0 in thin films of TPD and

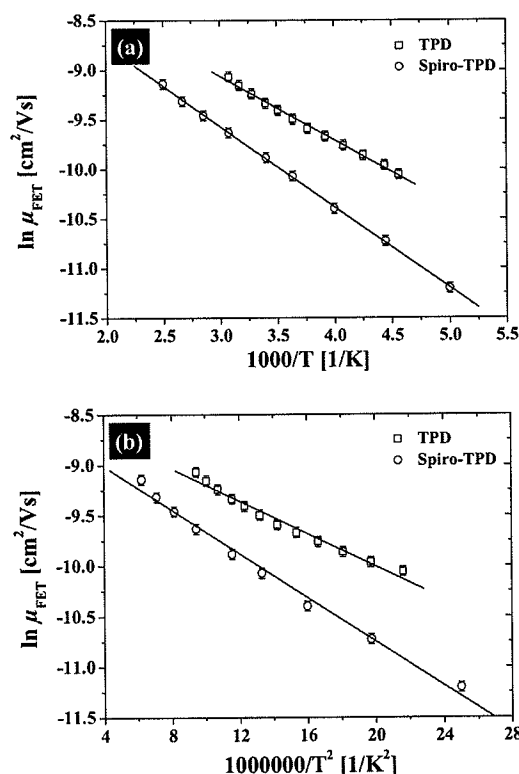


Figure 8. Field-effect mobilities of charge carriers in thin films of TPD and spiro-TPD plotted against a) the reciprocal of the temperature in the Arrhenius representation and b) the inverse square of the temperature in the GD Model.

spiro-TPD of 8×10^{-4} and $2 \times 10^{-4} \text{ cm}^2 \text{ V}^{-1} \text{ s}^{-1}$ were obtained for the Arrhenius and the GD model, respectively. Moreover, an activation energy, E_a , of 0.057 eV was obtained from the Arrhenius model for TPD, which is in contrast to the result obtained from the TOF technique ($E_a = 0.12 \text{ eV}$).^[19]

Figure 9a shows the temperature dependence of the field-effect mobility for a spiro-TPD FET at different gate biases ($V_G = -2.5, -10, -15, -20$, and -30 V). The lines are least-squares fits used to extract the E_a . Figure 9b shows the dependency of the activation energy on the applied gate bias. The apparent activation energy decreases with increasing gate bias. At low gate bias, E_a is large and, finally, saturates at a value of 0.050 eV as the gate bias is increased. The decrease of the activation energy with increasing absolute gate bias value is probably a result of accumulated charges filling the lower-lying states. Therefore, any additional charge carriers will occupy sites with a higher energy and less energy will be required for jumping to neighboring sites.^[29,30]

Table 4 summarizes all parameters that have been extracted from FET techniques. The prefactor mobilities obtained from the Arrhenius model for TAD, TPD, TTB, α -NPB, spiro-TAD, spiro-TTB, spiro-TPD, and spiro- α -NPB cover a broad range of 8.0×10^{-4} to $33 \text{ cm}^2 \text{ V}^{-1} \text{ s}^{-1}$, which is rather unexpected. In contrast, the prefactor mobilities obtained from the GD model cover a range from 2.0×10^{-4} to $4.5 \times 10^{-2} \text{ cm}^2 \text{ V}^{-1} \text{ s}^{-1}$, which is

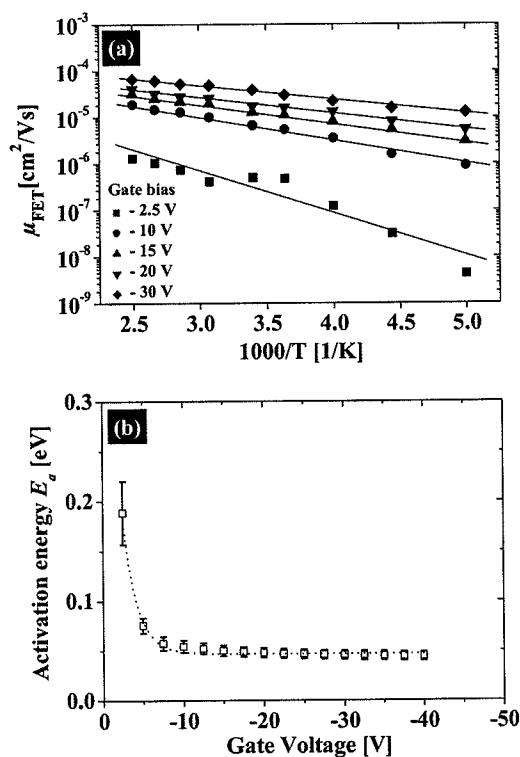


Figure 9. a) Temperature dependence of field-effect mobility for a spiro-TPD at gate biases of -2.5 V , -10 V , -15 V , -20 V , and -30 V and b) E_a of field-effect mobility plotted against gate voltage.

Table 4. Transport parameters extracted from the FET technique.

Material	Arrhenius model		Gaussian disorder model	
	μ_0 [$\text{cm}^2 \text{ V}^{-1} \text{ s}^{-1}$]	E_a [eV]	μ_0 [$\text{cm}^2 \text{ V}^{-1} \text{ s}^{-1}$]	σ [a] [eV]
TAD	7.6×10^{-2}	0.220	4.4×10^{-3}	0.077
Spiro-TAD	4.0×10^{-3}	0.110	4.0×10^{-4}	0.057
TPD	8.0×10^{-4}	0.057	2.0×10^{-4}	0.045
Spiro-TPD	8.0×10^{-4}	0.071	2.0×10^{-4}	0.051
TTB	33	0.330	4.5×10^{-2}	0.092
Spiro-TTB	0.2	0.206	3.3×10^{-3}	0.076
α -NPB	5.0×10^{-2}	0.174	2.0×10^{-3}	0.071
Spiro- α -NPB	8.0×10^{-2}	0.205	3.0×10^{-3}	0.077

[a] σ is the Gaussian distribution width.

realistic for amorphous thin films of low-molecular-weight materials. The Gaussian distribution widths, σ , obtained from the Gaussian disorder model for all films are in the range of 0.051 to 0.092 eV. The discrepancy between the good data fit and the large deviation in the prefactor mobility value for the Arrhenius model is not fully understood yet. However, we find that the temperature dependences of spiro-triarylamino compounds are slightly different from those of the parent compounds.

Based on our experimental data we conclude that the spiro concept influences the hole-transport properties of the parent compounds. In the case of symmetrically spiro-linked com-

pounds, the molecules have two identical chromophores connected through a central carbon atom. The chromophores are forced into a perpendicular arrangement by this linkage, resulting in a weak interaction of the molecular halves. In organic transistors based on symmetrically spiro-linked compounds, the active films contain radical cations that create the accumulation layer as the negative bias is applied to the gate electrode. A current between source and drain will flow if a bias is applied to the drain contact and the charges are mobile and not trapped. Since the transport is governed by a hopping mechanism, the charges in thin films of symmetrically spiro-linked compounds do not move as effectively as they can in the parent compounds. We conjecture that the hopping charges in thin films of symmetrically spiro-linked compounds probably take a longer path than those in thin films of the parent compounds. The reason is the symmetrically spiro-linked compounds contain two identical moieties and only one half of the molecule is active in the charge transport. Therefore, the charge-carrier mobilities in thin films of the parent compounds are slightly higher than those in thin films of the symmetrically spiro-linked compounds. However, we notice that the charge-carrier mobility in thin films of spiro-TTB is higher than that in TTB, because the TTB film is the most unstable among the parent compounds. We have also observed that the change of charge carriers in thin films of spiro-TTB is the largest among the symmetrically spiro-linked compound. Those observations are not fully understood at the moment, but we believe that the chemical structure of the compounds plays an important role in their stability. Therefore, the introduction of the spiro center between two identical moieties strongly improves the morphological stability of the corresponding thin films. However, we cannot generalize the difference between charge transport in thin films of symmetrically spiro-linked compounds and their corresponding parent compounds.

3. Conclusions

We have investigated the charge-transport properties of spiro-linked compounds and their corresponding parent compounds. We found that the hole mobilities in fresh thin films of spiro-linked compounds are of the same order of magnitude as those of the corresponding parent compounds. However, the transistor action of the parent compounds vanished after the sample was stored in an ambient atmosphere for several days because of the thin films' lack of morphological stability. In contrast, the hole mobilities of the spiro-linked compounds did not change significantly after the samples were stored in an ambient atmosphere up to nine months. From the temperature-dependence measurements, it has been found that the Arrhenius model provides a better fit of the experimental data. There are significant differences in the fit parameters for the spiro-linked compounds compared with their parent compounds. Therefore, the spiro concept, which is designed to improve the morphological stability, influences the charge-transport properties of the resulting compound.

4. Experimental

FETs were fabricated on p-Si as the substrate and the gate contact. A high-quality SiO₂ gate dielectric with a capacitance per unit area in the range of 17 to 20 nF cm⁻² was prepared by thermal oxidation in a dry oxygen atmosphere. Gold source and drain electrodes with 10 nm Ti adhesion layers were defined using standard photolithography with channel lengths varying between 2 and 10 μm and channel widths of between 2 and 5 mm. All spiro-linked compounds used in this study were synthesized by members of our group [16]. TPD (Product Number: 44 326-3, 99 %) was purchased from Aldrich Co., TAD (ST 16/5-04990.03), TTB (ST 16/3-03541.01), and α-NPB (ST 16/7-04264.02) were purchased from Sensient Imaging Technologies GmbH (Wolfen, Germany), and their purity was specified as higher than 99 %. These materials were used without further purification.

Prior to deposition of the active materials, the predefined substrates were cleaned by soaking in acetone, followed by oxygen-plasma treatment, and exposure to hexamethyldisilazane to replace the natural hydroxyl end group of the SiO₂ substrate with an apolar methoxy group. Finally, the active material was deposited by thermal evaporation at a vacuum of 10⁻⁶ Torr (1 Torr = 133 Pa) ($T_{\text{substrate}} \approx 298$ K, deposition rate = 0.04–0.1 nm s⁻¹) with a typical thicknesses in the range 100 to 150 nm. The transistor characteristics were measured utilizing a Keithley 4200 semiconductor characterization system equipped with a Keithley 4200 PA preamplifier for improved low-current measurement. Furthermore, all electrical characterizations performed with the Keithley 4200 were set up with a hold time of 0 s and a sweep delay of 100 ms [10]. The mobility in the linear regime was calculated from the slope of the plot of the I_D versus V_G according to $I_D = (W/L)\mu_{\text{FET}}C_i [V_D(V_G - V_T) - V_D^2/2]$, where V_T and μ_{FET} are the threshold voltage and field-effect mobility, respectively. On the other hand, the mobility in the saturation regime was calculated from the slope of the plot of the square root of the saturated drain current versus V_G according to $I_D = [W/(2L)]\mu_{\text{FET}}C_i(V_G - V_T)^2$ [31]. All samples were kept in an ambient atmosphere (22 °C, relative humidity of 24 %, in the dark). The AFM images of thin films were recorded with a Digital Instruments Nanoscope Multimode III using a scan frequency of between 0.5 and 2.0 Hz. Conducting silicon cantilevers (Nanosensors GmbH and NACATEC GmbH) with a spring constant of 41–46 N m⁻¹ and a resonance frequency of 340–390 kHz were used.

Received: June 10, 2005

Final version: July 22, 2005

Published online: April 12, 2006

- [1] S. A. Van Slyke, C. H. Chen, C. W. Tang, *Appl. Phys. Lett.* **1996**, *69*, 2160.
- [2] Y. Shirota, *J. Mater. Chem.* **2000**, *10*, 1.
- [3] C. D. Dimitrakopoulos, P. R. L. Malenfant, *Adv. Mater.* **2002**, *14*, 99.
- [4] J. Salbeck, in *Proc. Symp. Inorg. Org. Electroluminescence (EL 1996)* (Eds: R. H. Mauch, H. E. Gumlich), Wissenschaft und Technik, Berlin, Germany **1996**, p. 243.
- [5] U. Bach, D. Lupo, P. Compère, J. E. Moser, F. Weissörtel, J. Salbeck, H. Spreitzer, M. Grätzel, *Nature* **1998**, *395*, 583.
- [6] J. Salbeck, N. Yu, J. Bauer, F. Weissörtel, H. Bestgen, *Synth. Met.* **1997**, *91*, 209.
- [7] F. Steuber, J. Staudigel, M. Stössel, J. Simmerer, A. Winnacker, H. Spreitzer, F. Weissörtel, J. Salbeck, *Adv. Mater.* **2000**, *12*, 130.
- [8] J. Huang, M. Pfeiffer, J. Blochwitz, A. Werner, J. Salbeck, S. Liu, K. Leo, *Jpn. J. Appl. Phys.* **2001**, *40*, 6630.
- [9] T. P. I. Saragi, R. Pudlich, T. Fuhrmann, J. Salbeck, *Mater. Res. Soc. Symp. Proc.* **2002**, *725*, 89.
- [10] T. P. I. Saragi, T. Fuhrmann-Lieker, J. Salbeck, *Synth. Met.* **2005**, *148*, 267.
- [11] T. P. I. Saragi, R. Pudlich, T. Fuhrmann, J. Salbeck, *Appl. Phys. Lett.* **2004**, *84*, 2334.

- [12] N. Johansson, J. Salbeck, J. Bauer, F. Weissörtel, P. Bröms, A. Andersson, W. R. Salaneck, *Synth. Met.* **1999**, *101*, 405.
- [13] J. Salbeck, M. Schörner, T. Fuhrmann, *Thin Solid Films* **2002**, *417*, 20.
- [14] T. Spehr, R. Pudzich, T. Fuhrmann, J. Salbeck, *Org. Electron.* **2003**, *4*, 61.
- [15] T. P. I. Saragi, *Ph.D. Thesis*, Universität Kassel, Germany **2004**.
- [16] F. Weissörtel, *Ph.D. Thesis*, Universität Regensburg, Germany **1999**.
- [17] E.-M. Han, L.-M. Do, M. Fujihara, H. Inada, Y. Shirota, *J. Appl. Phys.* **1996**, *80*, 3297.
- [18] S. Heun, P. Borsenberger, *Chem. Phys.* **1995**, *200*, 245.
- [19] M. Stolka, J. F. Yanus, D. M. Pai, *J. Phys. Chem.* **1984**, *88*, 4707.
- [20] H. H. Fong, K. C. Lun, S. K. So, *Chem. Phys. Lett.* **2002**, *353*, 407.
- [21] P. M. Borsenberger, J. J. Fitzgerald, *J. Phys. Chem.* **1993**, *97*, 4815.
- [22] N. von Malm, *Ph.D. Thesis*, Technische Universität Darmstadt, Germany **2003**.
- [23] B. Chen, C.-S. Lee, S.-T. Lee, P. Webb, Y.-C. Chan, W. Gambling, H. Tian, W. Zhu, *Jpn. J. Appl. Phys.* **2000**, *39*, 1190.
- [24] M. Iizuka, N. Nakamura, K. Kudo, K. Tanaka, *IEICE Trans. Electron.* **2002**, *E85-C*, 1311.
- [25] J. Kovac, T. C. Wong, M. K. Fung, M. W. Liu, V. Kremnican, I. Bello, S. T. Lee, *Mater. Sci. Eng. B* **2001**, *85*, 172.
- [26] W. D. Gill, *J. Appl. Phys.* **1972**, *43*, 5033.
- [27] H. Bässler, *Phys. Status Solidi B* **1993**, *175*, 15.
- [28] P. M. Borsenberger, D. S. Weiss, *Organic Photoreceptors for Imaging Systems*, Marcel Dekker, New York **1993**.
- [29] A. R. Brown, C. P. Jarrett, D. M. de Leeuw, M. Matters, *Synth. Met.* **1997**, *88*, 37.
- [30] M. C. J. M. Vissenberg, M. Matters, *Phys. Rev. B: Condens Matter* **1998**, *57*, 12 964.
- [31] S. M. Sze, *Physics of Semiconductor Devices*, Wiley, New York **1981**.